Stern-Volmer Experiments with $[Ru(bpy)_3]^{2+}$

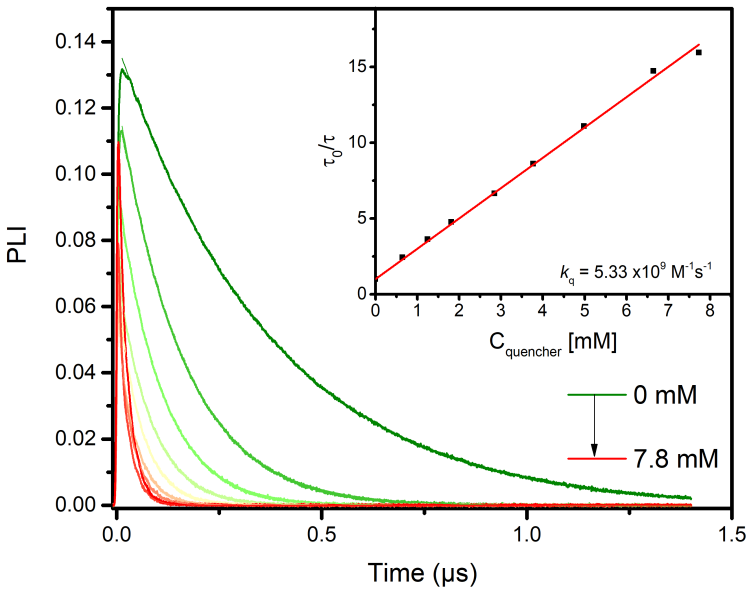

Figure S1. Excited-state quenching of $[Ru(bpy)_3]^{2+}$ in the presence of increasing amounts of 4-bromo-benzene-diazonium tetrafluoroborate. Experiments were carried out in argon purged CH_3CN containing 0.1M $TBABF_4$. The inset represents the Stern-Volmer plot from which the quenching rate constant (k_q) was determined.

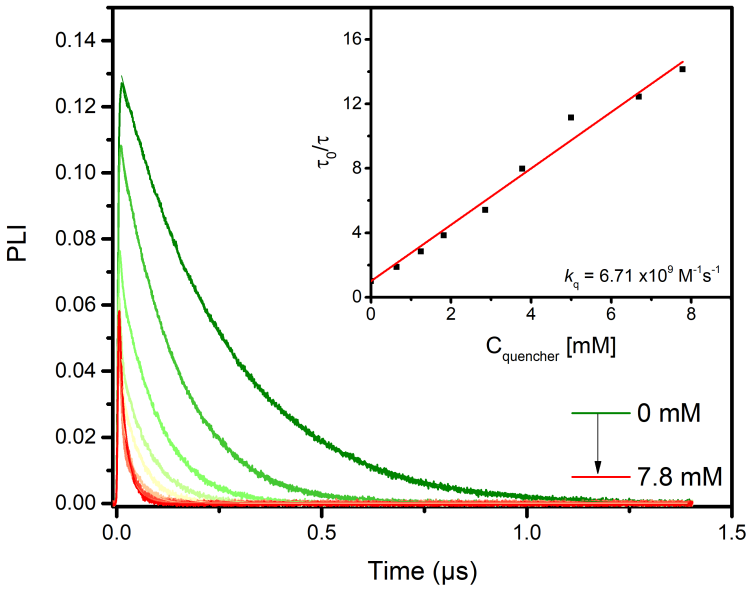

Figure S2. Excited-state quenching of $[Ru(bpy)_3]^{2+}$ in the presence of increasing amounts of 4-CF_3-benzene-diazonium tetrafluoroborate. Experiments were carried out in argon purged CH_3CN containing 0.1M $TBABF_4$. The inset represents the Stern-Volmer plot from which the quenching rate constant (k_q) was determined.

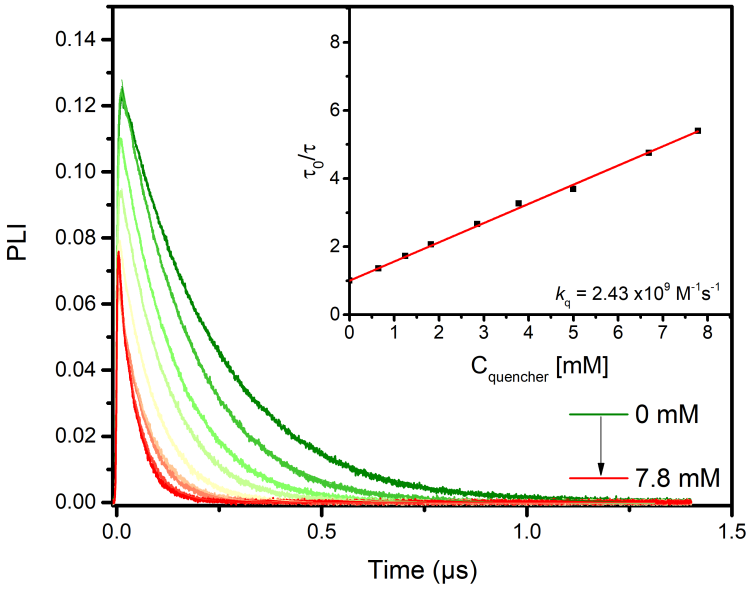

Figure S3. Excited-state quenching of $[Ru(bpy)_3]^{2+}$ in the presence of increasing amounts of 4-carboxylate-benzene-diazonium. Experiments were carried out in argon purged CH_3CN containing 0.1M $TBABF_4$. The inset represents the Stern-Volmer plot from which the quenching rate constant (k_q) was determined.

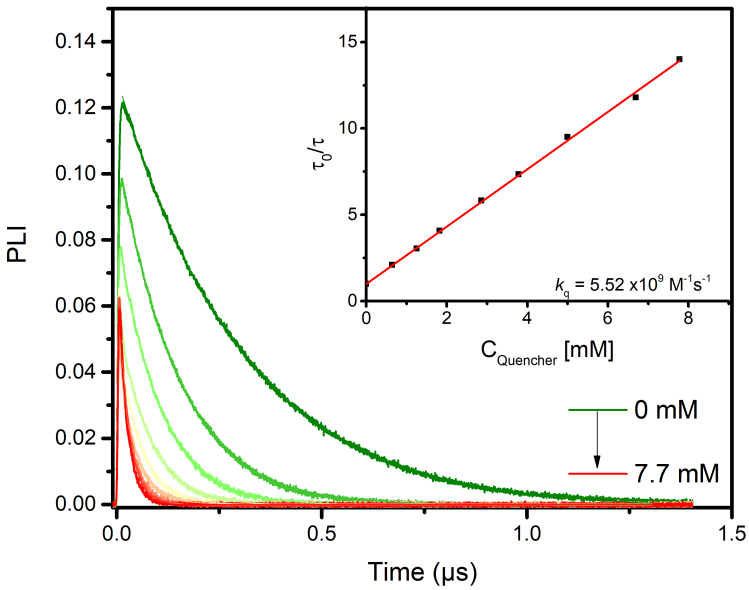

Figure S4. Excited-state quenching of $[Ru(bpy)_3]^{2+}$ in the presence of increasing amounts of 4-ethylester-benzene-diazonium tetrafluoroborate. Experiments were carried out in argon purged CH_3CN containing 0.1M $TBABF_4$. The inset represents the Stern-Volmer plot from which the quenching rate constant (k_q) was determined.

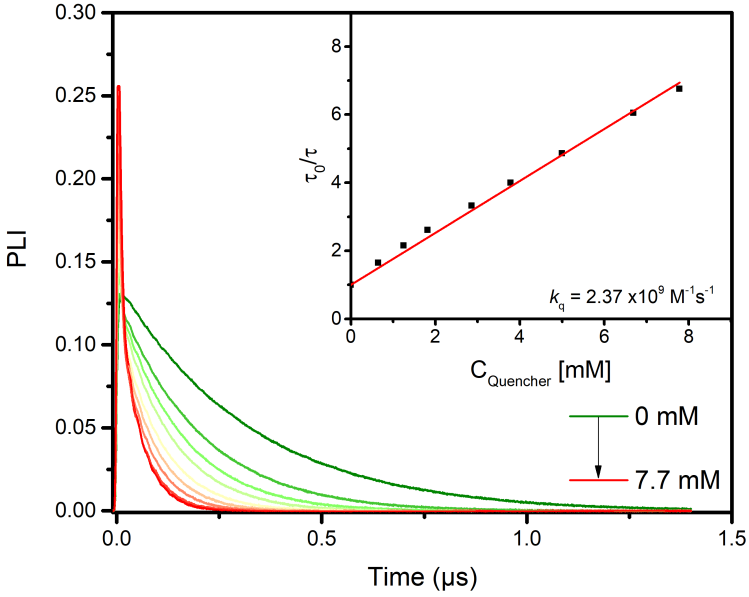

Figure S5. Excited-state quenching of $[Ru(bpy)_3]^{2+}$ in the presence of increasing amounts of 4-cyclohexyl-benzene-diazonium tetrafluoroborate. Experiments were carried out in argon purged CH_3CN containing 0.1M $TBABF_4$. The inset represents the Stern-Volmer plot from which the quenching rate constant (k_q) was determined.

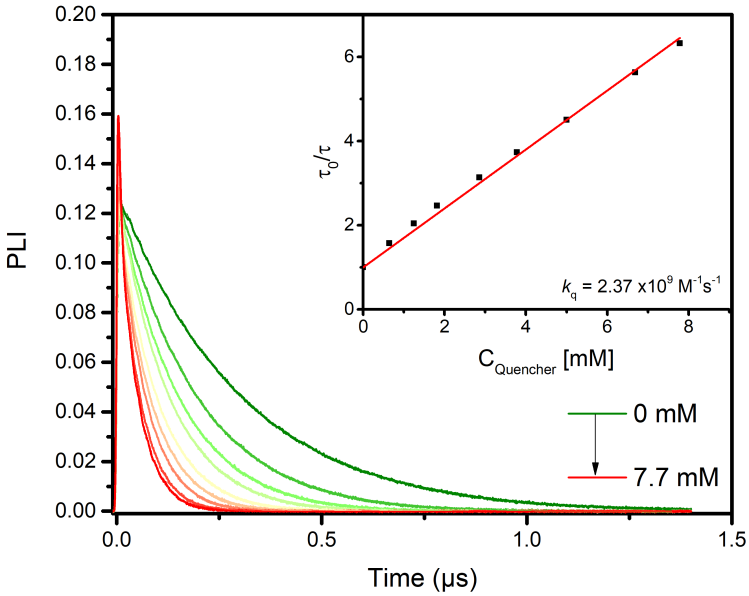

Figure S6. Excited-state quenching of $[Ru(bpy)_3]^{2+}$ in the presence of increasing amounts of 4-ethyl-benzene-diazonium tetrafluoroborate. Experiments were carried out in argon purged CH_3CN containing 0.1M $TBABF_4$. The inset represents the Stern-Volmer plot from which the quenching rate constant (k_q) was determined.

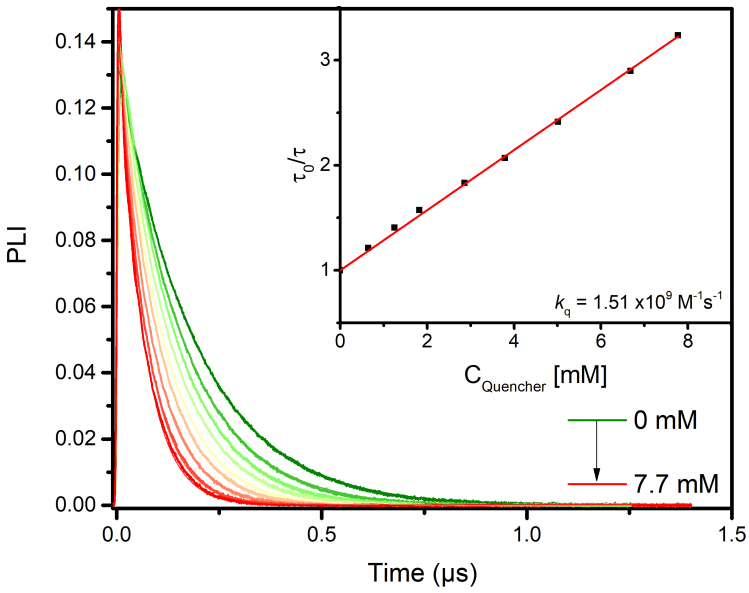

Figure S7. Excited-state quenching of $[Ru(bpy)_3]^{2+}$ in the presence of increasing amounts of 4-methoxy-benzene-diazonium tetrafluoroborate. Experiments were carried out in argon purged CH_3CN containing 0.1M $TBABF_4$. The inset represents the Stern-Volmer plot from which the quenching rate constant (k_q) was determined.

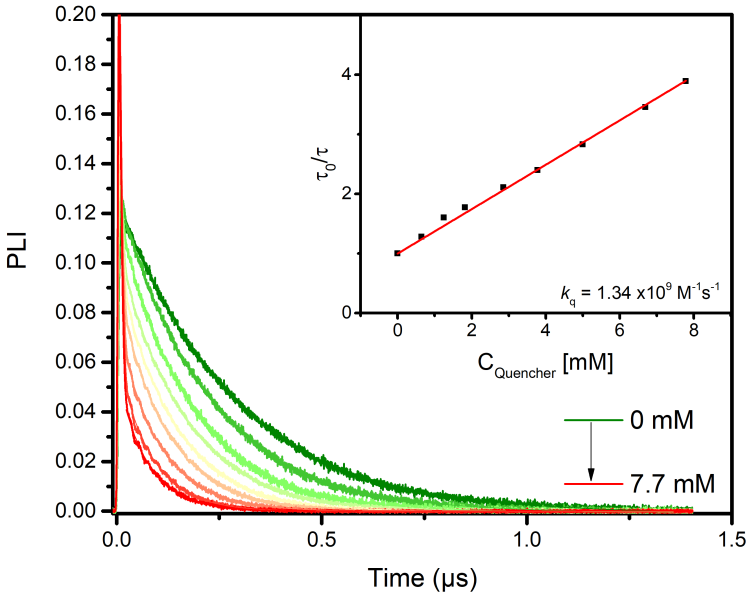

Figure S8. Excited-state quenching of $[Ru(bpy)_3]^{2+}$ in the presence of increasing amounts of 4-(N,N)-diethylamine- benzene-diazonium tetrafluoroborate. Experiments were carried out in argon purged CH_3CN containing 0.1M $TBABF_4$. The inset represents the Stern-Volmer plot from which the quenching rate constant (k_q) was determined.

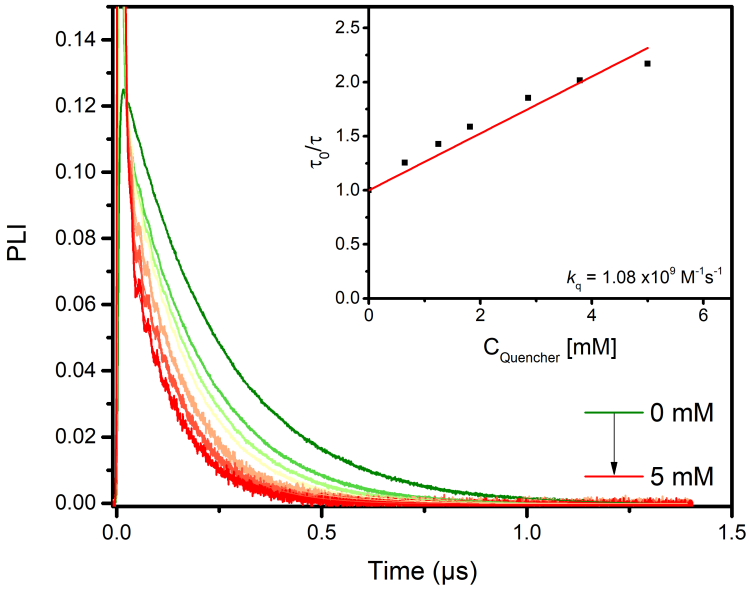

Figure S9. Excited-state quenching of $[Ru(bpy)_3]^{2+}$ in the presence of increasing amounts of 4(N,N)-dimethylamine -benzene-diazonium tetrafluoroborate. Experiments were carried out in argon purged CH_3CN containing 0.1M $TBABF_4$. The inset represents the Stern-Volmer plot from which the quenching rate constant (k_q) was determined.

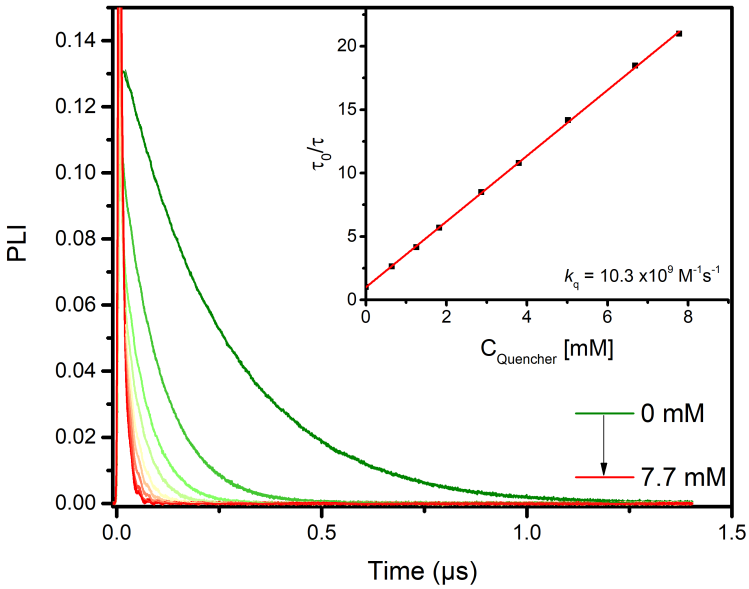

Figure S10. Excited-state quenching of $[Ru(bpy)_3]^{2+}$ in the presence of increasing amounts of 4-nitro-benzene-diazonium tetrafluoroborate. Experiments were carried out in argon purged CH_3CN containing 0.1M $TBABF_4$. The inset represents the Stern-Volmer plot from which the quenching rate constant (k_q) was determined.

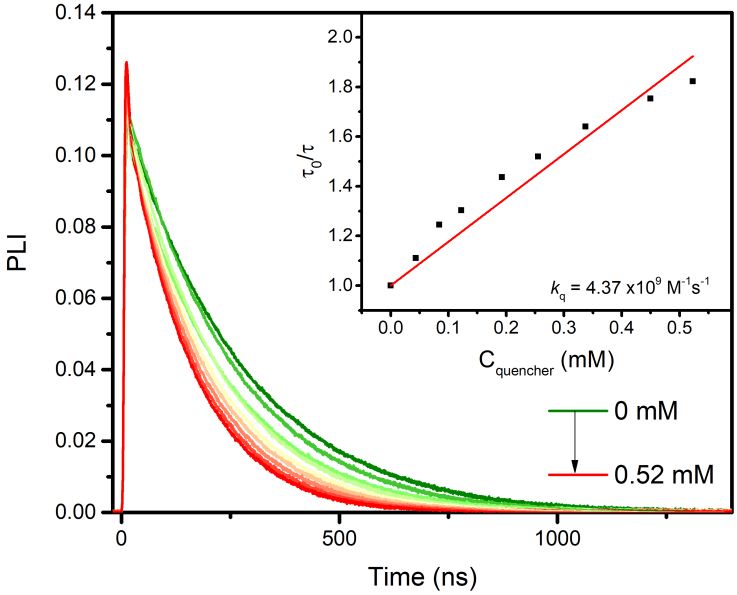

Figure S11. Excited-state quenching of $[Ru(bpy)_3]^{2+}$ in the presence of increasing amounts **X₄-A**. Experiments were carried out in argon purged CH_3CN containing 0.1M $TBABF_4$. The inset represents the Stern-Volmer plot from which the quenching rate constant (k_q) was determined. The linear relationship does not adequately fit the data but was used to provide an estimate of the range of quenching rate constant. Deviation from linearity is particularly prominent at higher concentration of quencher, where permanent photochemistry is more noticeable.

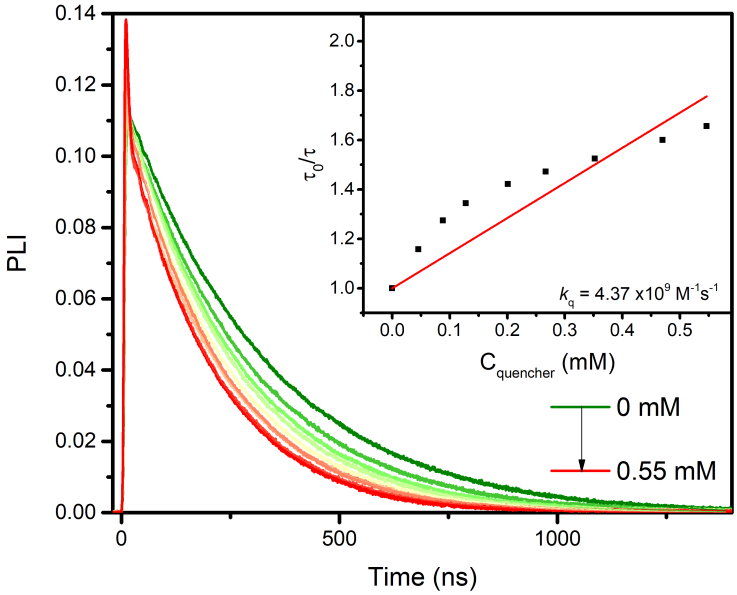

Figure S12. Excited-state quenching of $[Ru(bpy)_3]^{2+}$ in the presence of increasing amounts **X₄-B**. Experiments were carried out in argon purged CH_3CN containing 0.1M $TBABF_4$. The inset represents the Stern-Volmer plot from which the quenching rate constant (k_q) was determined. The linear relationship does not adequately fit the data but was used to provide an estimate of the range of quenching rate constant. Deviation from linearity is particularly prominent at higher concentration of quencher, where permanent photochemistry is more noticeable.

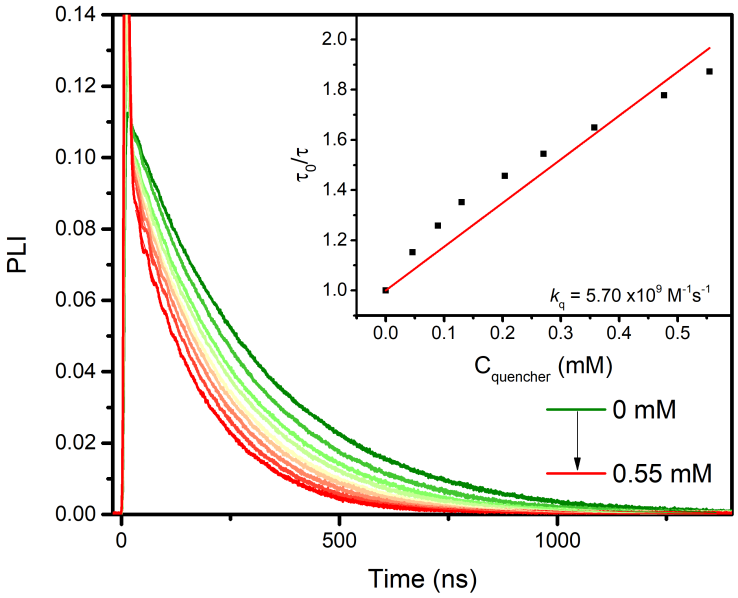

Figure S13. Excited-state quenching of $[Ru(bpy)_3]^{2+}$ in the presence of increasing amounts **X$_4$-C**. Experiments were carried out in argon purged CH_3CN containing 0.1M $TBABF_4$. The inset represents the Stern-Volmer plot from which the quenching rate constant (k_q) was determined. The linear relationship does not adequately fit the data but was used to provide an estimate of the range of quenching rate constant. Deviation from linearity is particularly prominent at higher concentration of quencher, where permanent photochemistry is more noticeable.

Stern-Volmer Experiments with $[Os(bpy)_3]^{2+}$

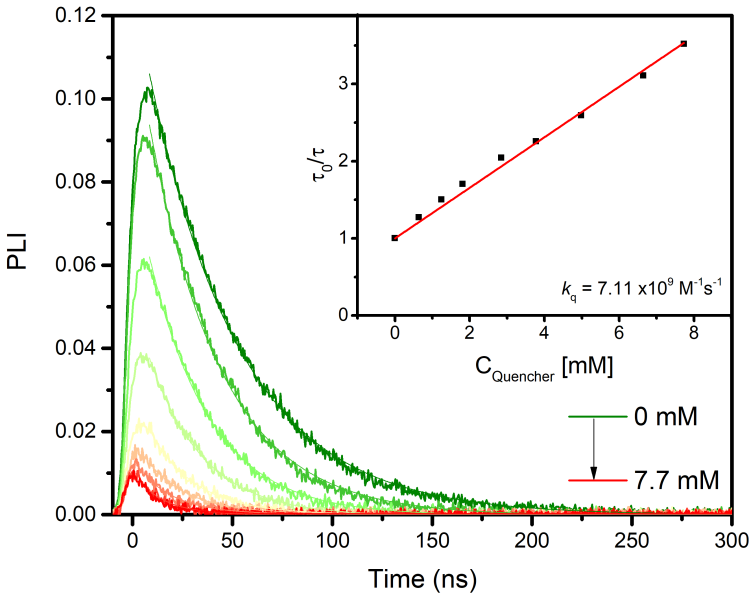

Figure S14. Excited-state quenching of $[Os(bpy)_3]^{2+}$ in the presence of increasing amounts of 4-bromo-benzene-diazonium tetrafluoroborate. Experiments were carried out in argon purged CH_3CN containing 0.1M $TBABF_4$. The inset represents the Stern-Volmer plot from which the quenching rate constant (k_q) was determined.

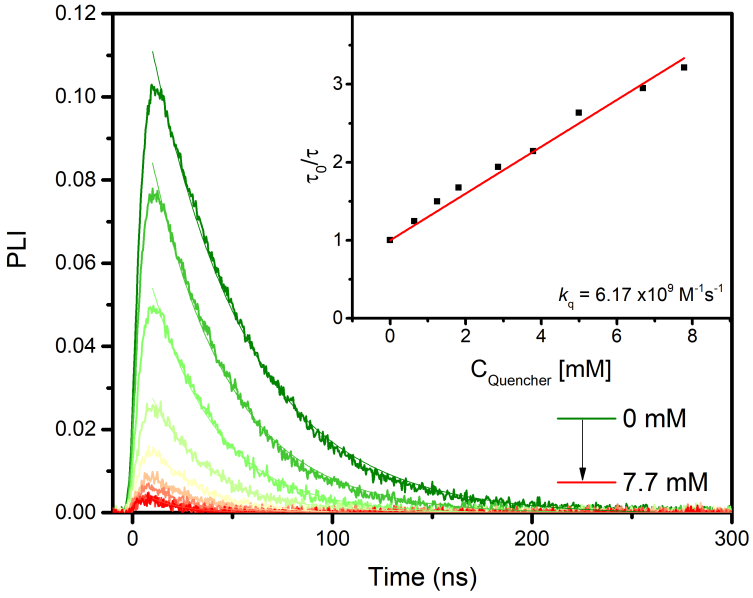

Figure S15. Excited-state quenching of $[Os(bpy)_3]^{2+}$ in the presence of increasing amounts of 4-CF_3-benzene-diazonium tetrafluoroborate. Experiments were carried out in argon purged CH_3CN containing 0.1M $TBABF_4$. The inset represents the Stern-Volmer plot from which the quenching rate constant (k_q) was determined.

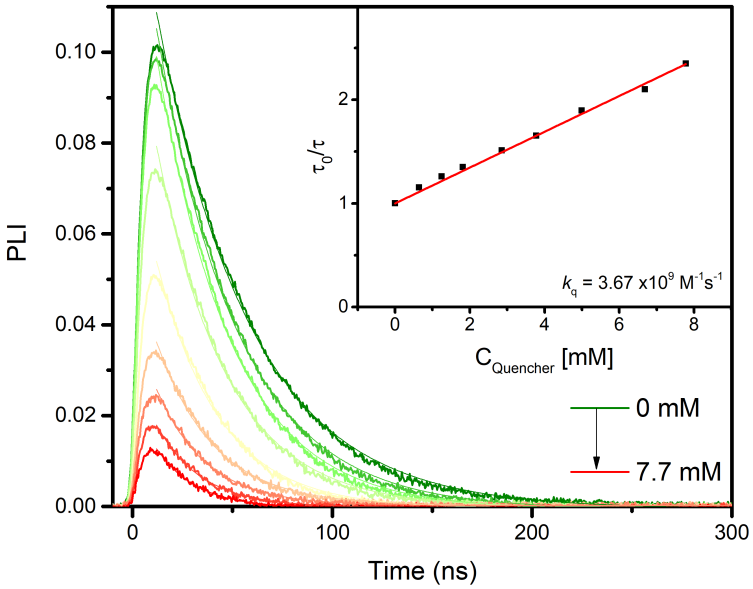

Figure S16. Excited-state quenching of $[Os(bpy)_3]^{2+}$ in the presence of increasing amounts of 4-carboxylate-benzene-diazonium. Experiments were carried out in argon purged CH_3CN containing 0.1M $TBABF_4$. The inset represents the Stern-Volmer plot from which the quenching rate constant (k_q) was determined.

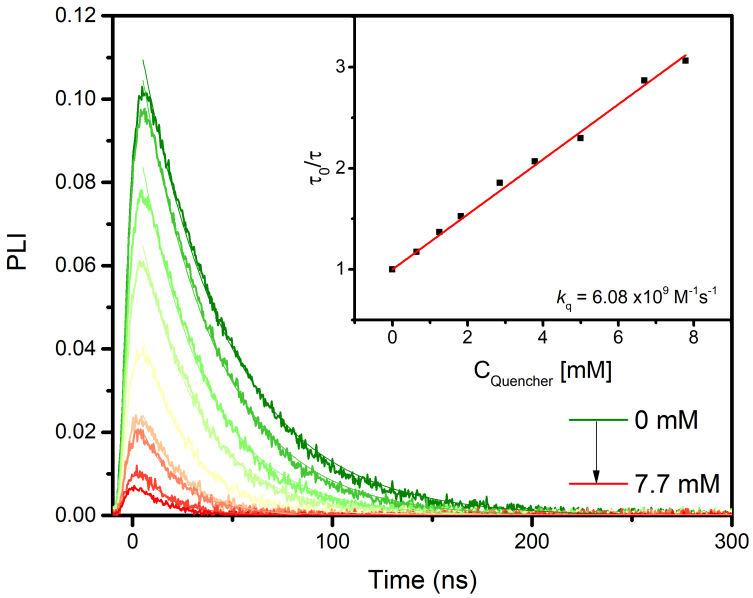

Figure S17. Excited-state quenching of $[Os(bpy)_3]^{2+}$ in the presence of increasing amounts of 4-ethylester-benzene-diazonium tetrafluoroborate. Experiments were carried out in argon purged CH_3CN containing 0.1M $TBABF_4$. The inset represents the Stern-Volmer plot from which the quenching rate constant (k_q) was determined.

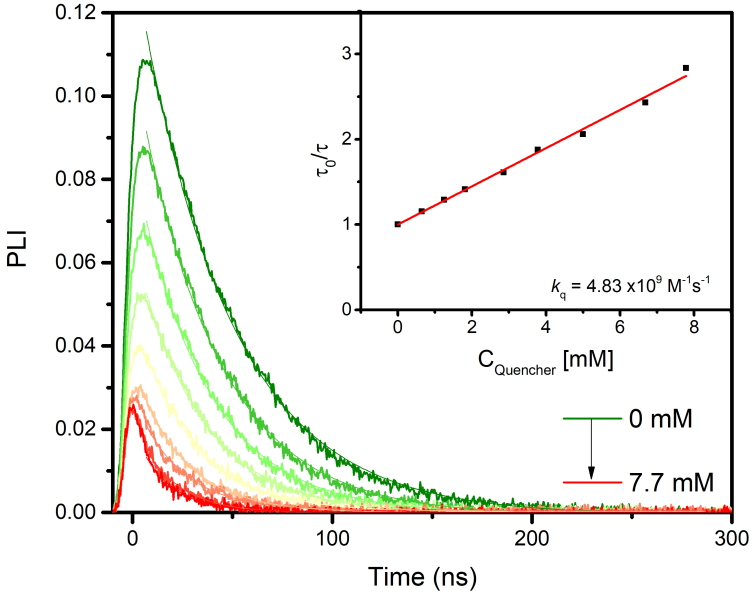

Figure S18. Excited-state quenching of $[Os(bpy)_3]^{2+}$ in the presence of increasing amounts of 4-cyclohexyl-benzene-diazonium tetrafluoroborate. Experiments were carried out in argon purged CH_3CN containing 0.1M $TBABF_4$. The inset represents the Stern-Volmer plot from which the quenching rate constant (k_q) was determined.

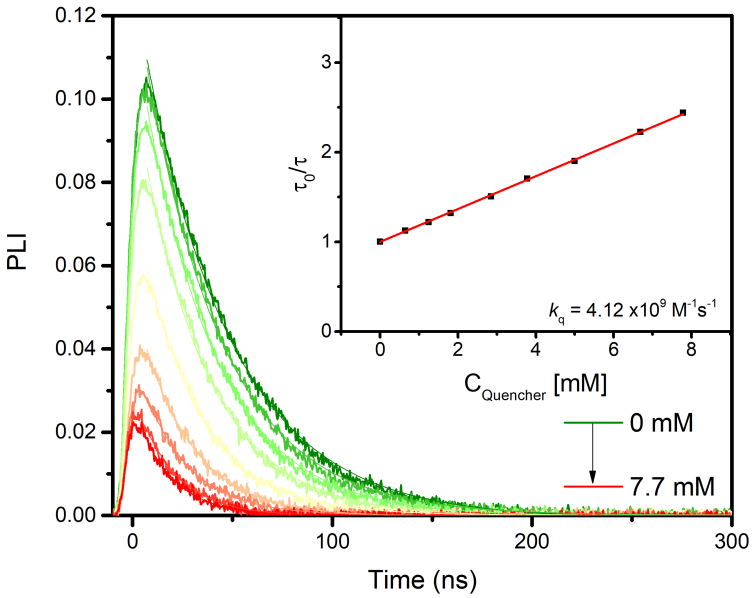

Figure S19. Excited-state quenching of $[Os(bpy)_3]^{2+}$ in the presence of increasing amounts of 4-ethyl-benzene-diazonium tetrafluoroborate. Experiments were carried out in argon purged CH_3CN containing 0.1M $TBABF_4$. The inset represents the Stern-Volmer plot from which the quenching rate constant (k_q) was determined.

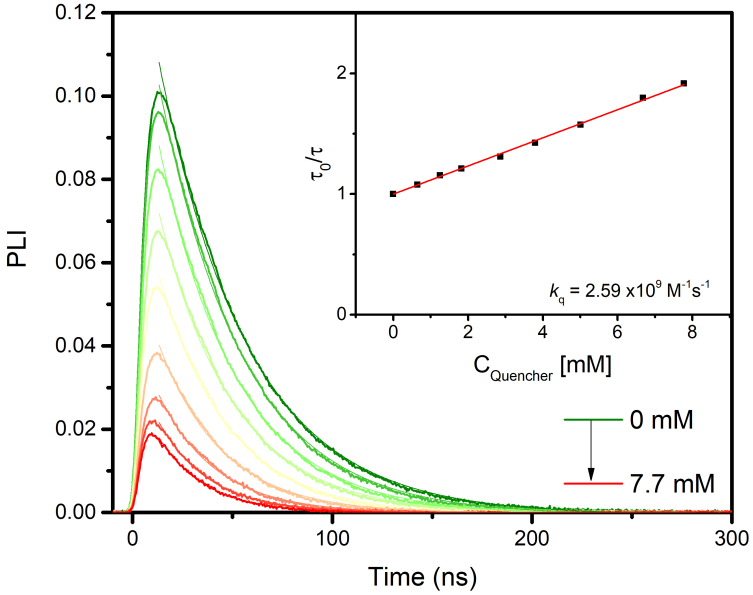

Figure S20. Excited-state quenching of $[Os(bpy)_3]^{2+}$ in the presence of increasing amounts of 4-methoxy-benzene-diazonium tetrafluoroborate. Experiments were carried out in argon purged CH_3CN containing 0.1M $TBABF_4$. The inset represents the Stern-Volmer plot from which the quenching rate constant (k_q) was determined.

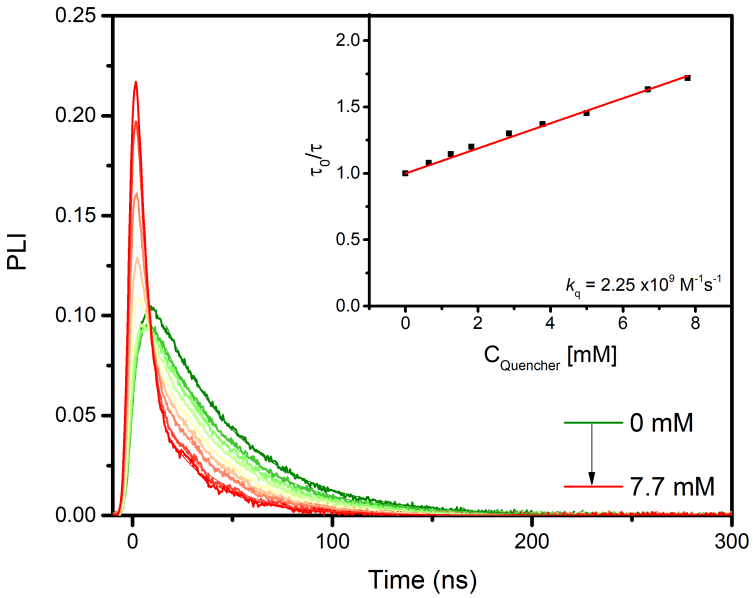

Figure S21. Excited-state quenching of $[Os(bpy)_3]^{2+}$ in the presence of increasing amounts of 4-(N,N)-diethylamine-benzene-diazonium tetrafluoroborate. Experiments were carried out in argon purged CH_3CN containing 0.1M $TBABF_4$. The inset represents the Stern-Volmer plot from which the quenching rate constant (k_q) was determined.

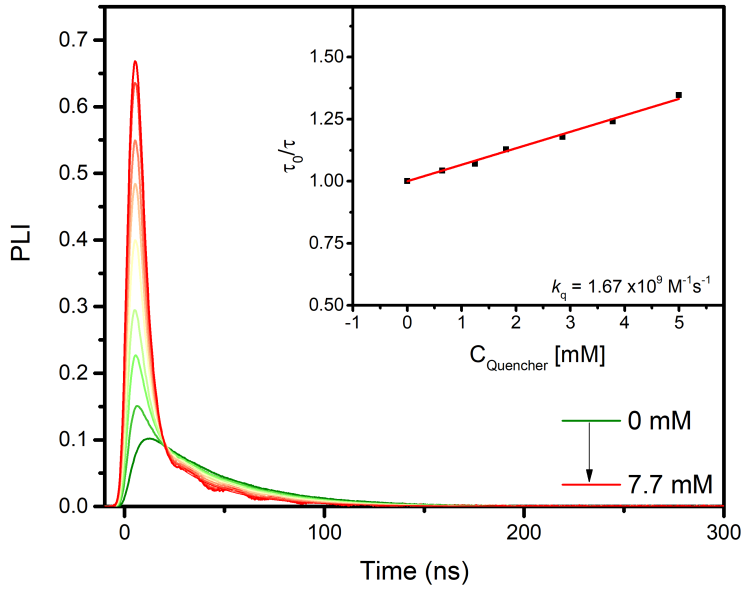

Figure S22. Excited-state quenching of $[Os(bpy)_3]^{2+}$ in the presence of increasing amounts of 4-(N,N)-dimethylamine-benzene-diazonium tetrafluoroborate. Experiments were carried out in argon purged CH_3CN containing 0.1M $TBABF_4$. The inset represents the Stern-Volmer plot from which the quenching rate constant (k_q) was determined.

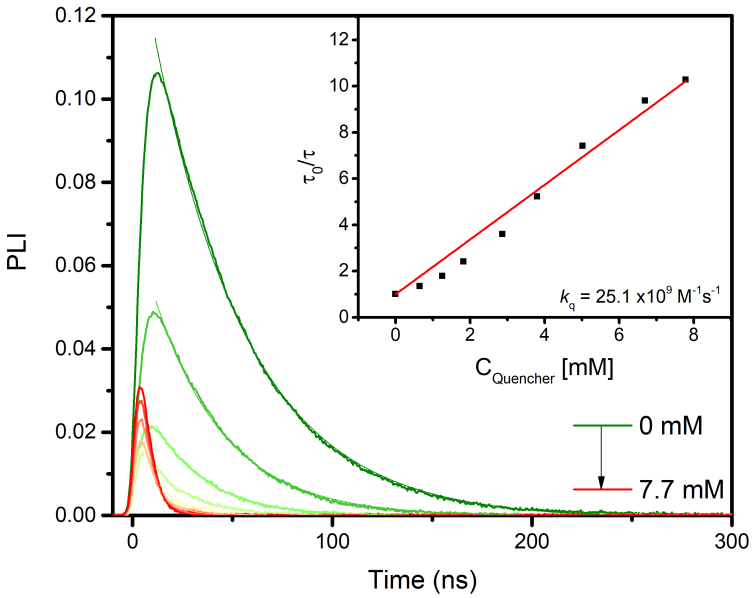

Figure S23. Excited-state quenching of $[Os(bpy)_3]^{2+}$ in the presence of increasing amounts of 4-nitro-benzene-diazonium tetrafluoroborate. Experiments were carried out in argon purged CH_3CN containing 0.1M $TBABF_4$. The inset represents the Stern-Volmer plot from which the quenching rate constant (k_q) was determined.

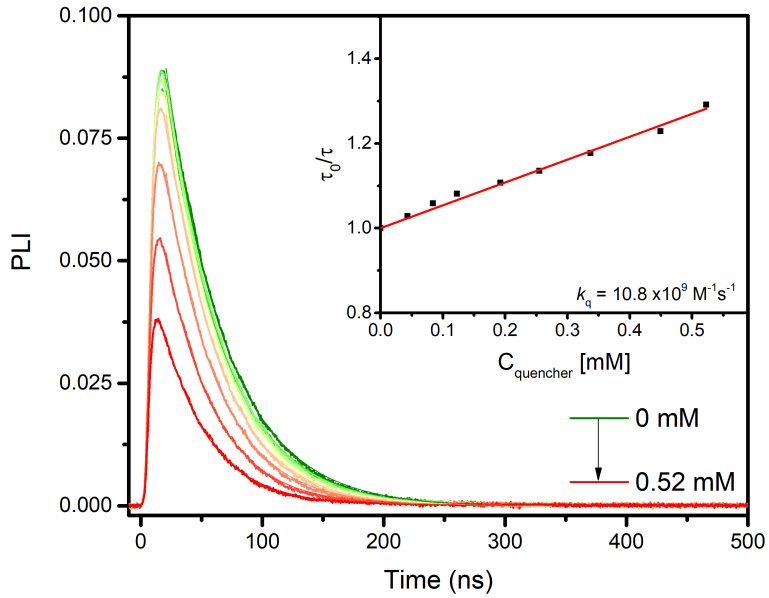

Figure S24. Excited-state quenching of $[Os(bpy)_3]^{2+}$ in the presence of increasing amounts of **X_4-A**. Experiments were carried out in argon purged CH_3CN containing 0.1M $TBABF_4$. The inset represents the Stern-Volmer plot from which the quenching rate constant (k_q) was determined.

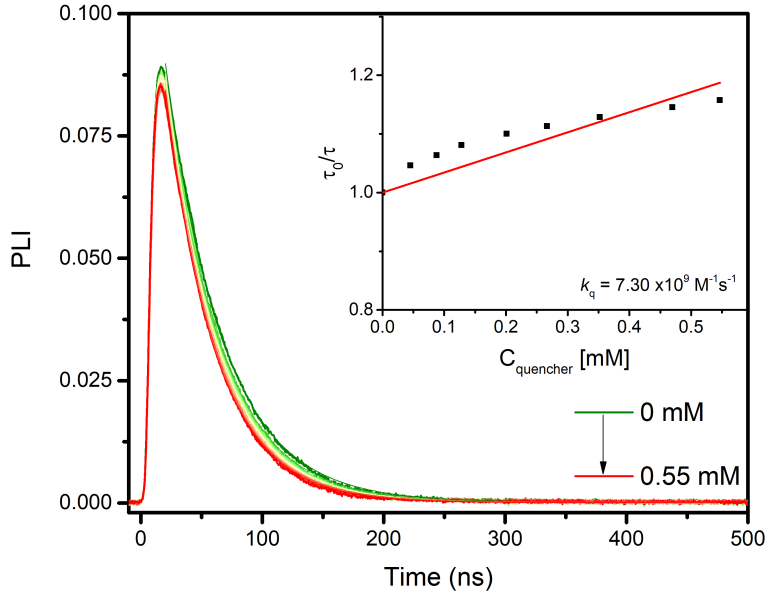

Figure S25. Excited-state quenching of $[Os(bpy)_3]^{2+}$ in the presence of increasing amounts of **X_4-B**. Experiments were carried out in argon purged CH_3CN containing 0.1M $TBABF_4$. The inset represents the Stern-Volmer plot from which the quenching rate constant (k_q) was determined. The linear relationship does not adequately fit the data but was used to provide an estimate of the range of quenching rate constant. Deviation from linearity is particularly prominent at higher concentration of quencher, where permanent photochemistry is more noticeable.

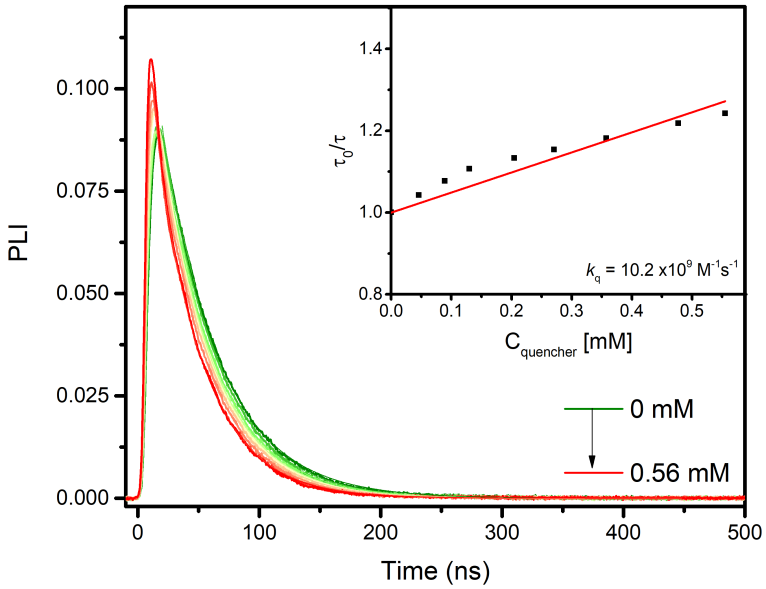

Figure S26. Excited-state quenching of $[Os(bpy)_3]^{2+}$ in the presence of increasing amounts **X_4-C**. Experiments were carried out in argon purged CH_3CN containing 0.1M $TBABF_4$. The inset represents the Stern-Volmer plot from which the quenching rate constant (k_q) was determined. The linear relationship does not adequately fit the data but was used to provide an estimate of the range of quenching rate constant. Deviation from linearity is particularly prominent at higher concentration of quencher, where permanent photochemistry is more noticeable.

Stern-Volmer Experiments with [Ir(ppy)$_3$]

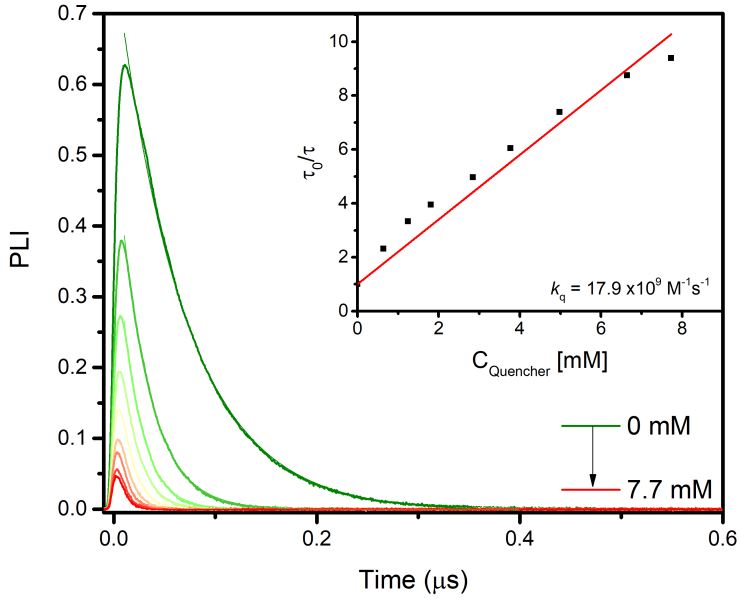

Figure S27. Excited-state quenching of [Ir(ppy)$_3$] in the presence of increasing amounts of 4-bromo-benzene-diazonium tetrafluoroborate. Experiments were carried out in argon purged CH_3CN containing 0.1M $TBABF_4$. The inset represents the Stern-Volmer plot from which the quenching rate constant (k_q) was determined.

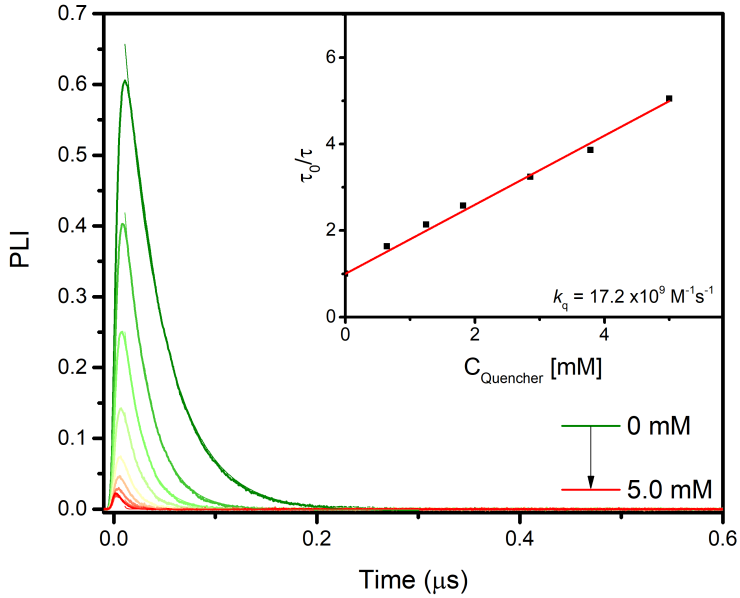

Figure S28. Excited-state quenching of [Ir(ppy)$_3$] in the presence of increasing amounts of 4-CF_3-benzene-diazonium tetrafluoroborate. Experiments were carried out in argon purged CH_3CN containing 0.1M $TBABF_4$. The inset represents the Stern-Volmer plot from which the quenching rate constant (k_q) was determined.

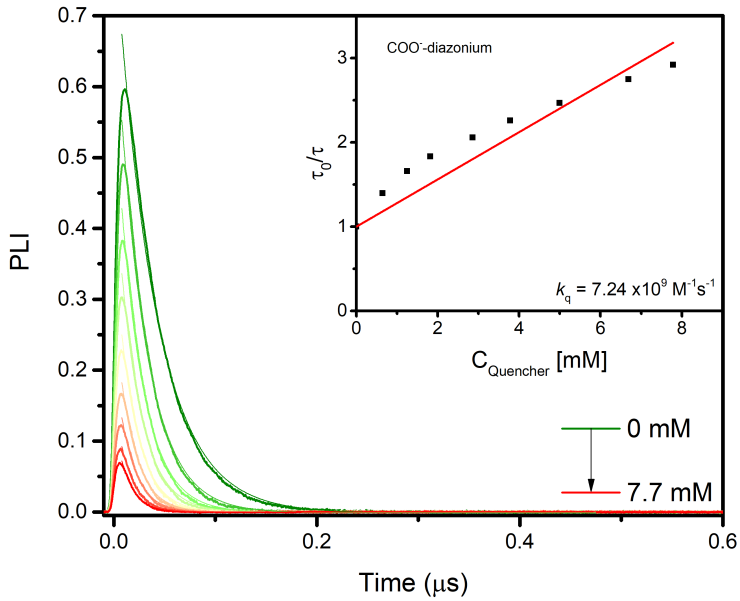

Figure S29. Excited-state quenching of [Ir(ppy)$_3$] in the presence of increasing amounts of 4-carboxylate-benzene-diazonium tetrafluoroborate. Experiments were carried out in argon purged CH_3CN containing 0.1M $TBABF_4$. The inset represents the Stern-Volmer plot from which the quenching rate constant (k_q) was determined.

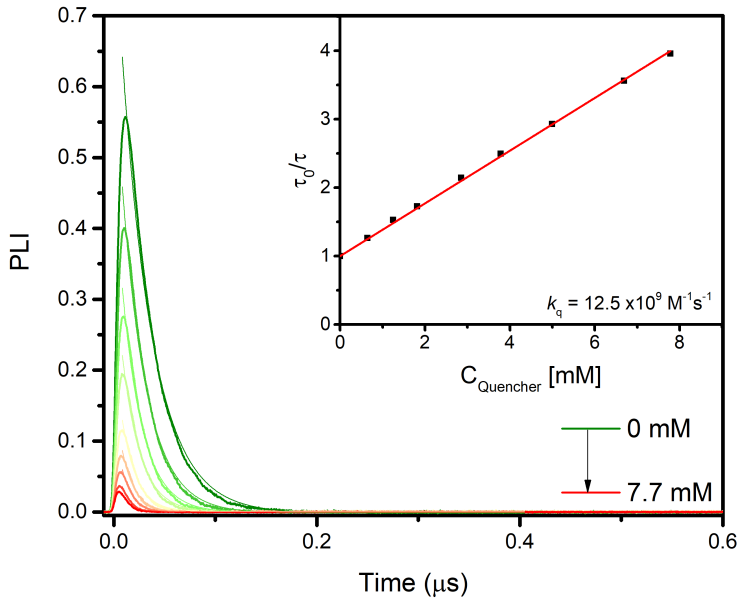

Figure S30. Excited-state quenching of [Ir(ppy)$_3$] in the presence of increasing amounts of 4-ethylester-benzene-diazonium tetrafluoroborate. Experiments were carried out in argon purged CH_3CN containing 0.1M $TBABF_4$. The inset represents the Stern-Volmer plot from which the quenching rate constant (k_q) was determined.

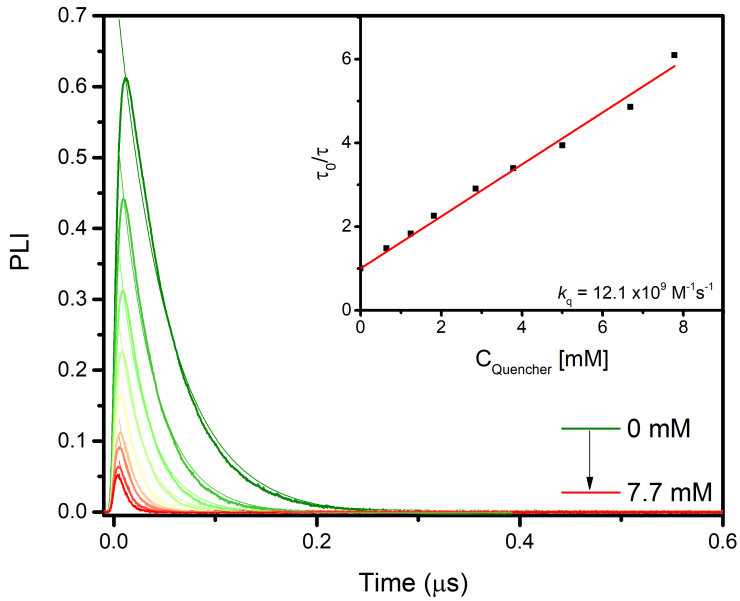

Figure S31. Excited-state quenching of [Ir(ppy)$_3$] in the presence of increasing amounts of 4-cyclohexyl-benzene-diazonium tetrafluoroborate. Experiments were carried out in argon purged CH_3CN containing 0.1M $TBABF_4$. The inset represents the Stern-Volmer plot from which the quenching rate constant (k_q) was determined.

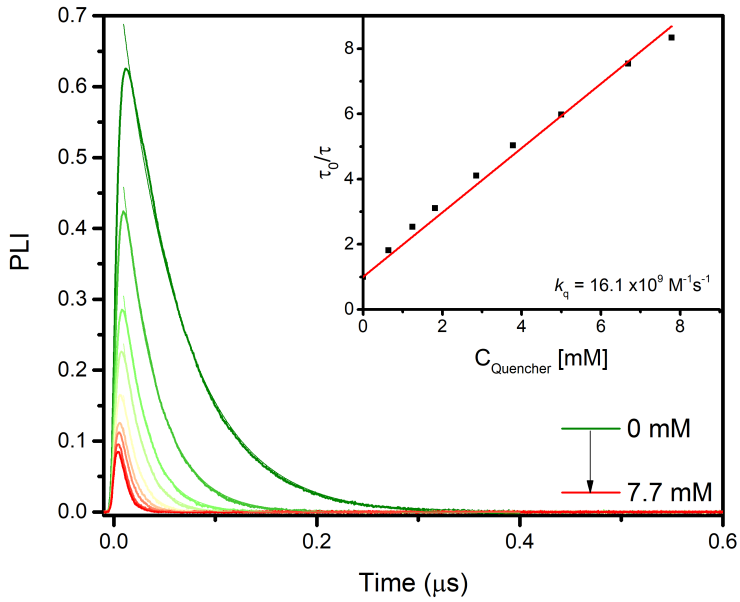

Figure S32. Excited-state quenching of [Ir(ppy)$_3$] in the presence of increasing amounts of 4-ethyl-benzene-diazonium tetrafluoroborate. Experiments were carried out in argon purged CH_3CN containing 0.1M $TBABF_4$. The inset represents the Stern-Volmer plot from which the quenching rate constant (k_q) was determined.

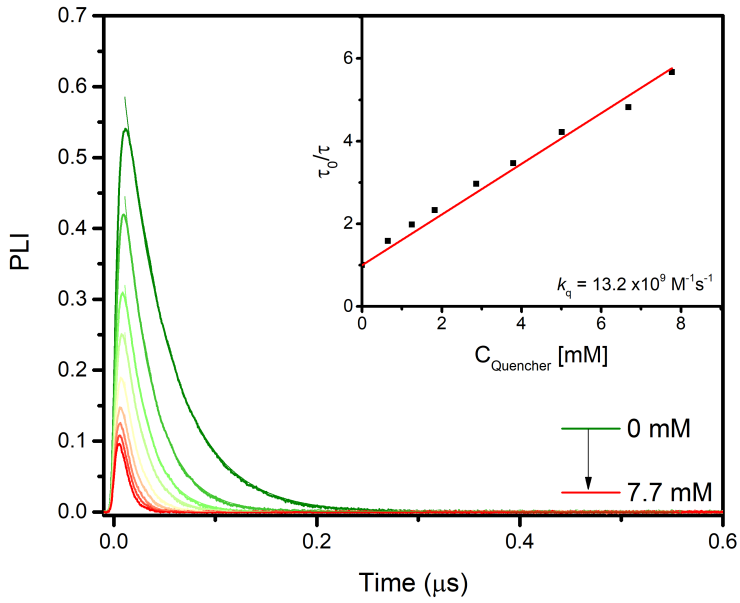

Figure S33. Excited-state quenching of [Ir(ppy)$_3$] in the presence of increasing amounts of 4-methoxy-benzene-diazonium tetrafluoroborate. Experiments were carried out in argon purged CH_3CN containing 0.1M $TBABF_4$. The inset represents the Stern-Volmer plot from which the quenching rate constant (k_q) was determined.

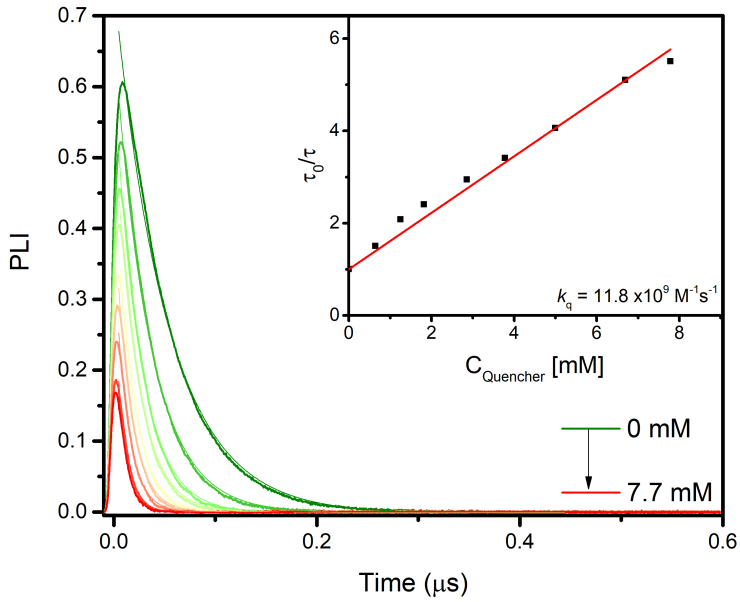

Figure S34. Excited-state quenching of [Ir(ppy)$_3$] in the presence of increasing amounts of 4-(N,N-diethylamine-benzene-diazonium tetrafluoroborate. Experiments were carried out in argon purged CH_3CN containing 0.1M $TBABF_4$. The inset represents the Stern-Volmer plot from which the quenching rate constant (k_q) was determined.

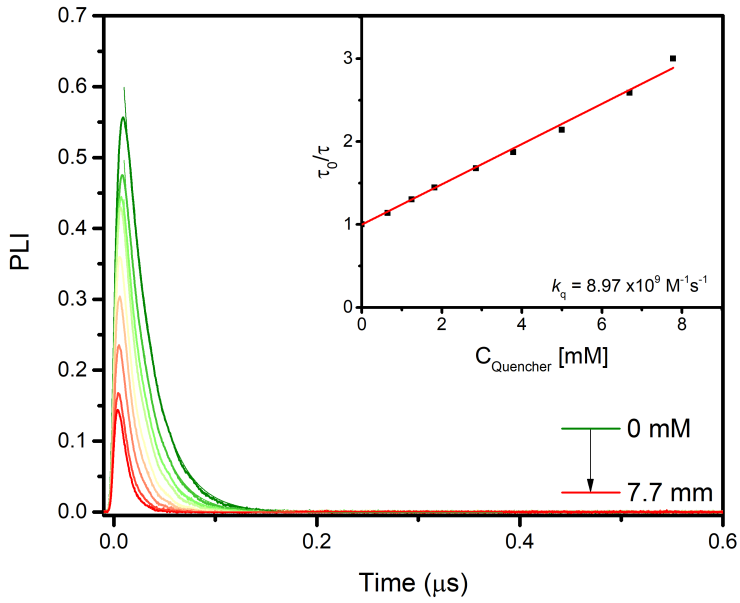

Figure S35. Excited-state quenching of [Ir(ppy)$_3$] in the presence of increasing amounts of 4-(N,N)-dimethylamine-benzene-diazonium tetrafluoroborate. Experiments were carried out in argon purged CH_3CN containing 0.1M $TBABF_4$. The inset represents the Stern-Volmer plot from which the quenching rate constant (k_q) was determined.

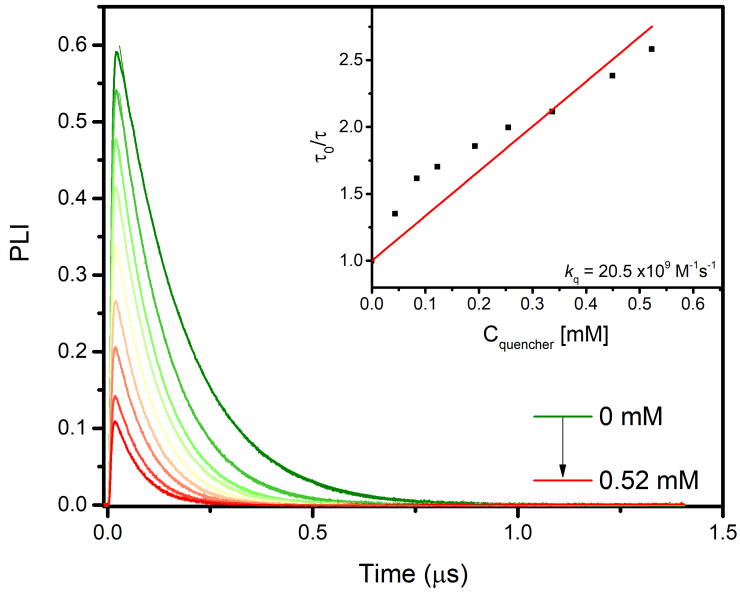

Figure S36. Excited-state quenching of [Ir(ppy)$_3$] in the presence of increasing amounts of **X$_4$-A**. Experiments were carried out in argon purged CH_3CN containing 0.1M $TBABF_4$. The inset represents the Stern-Volmer plot from which the quenching rate constant (k_q) was determined. The linear relationship does not adequately fit the data but was used to provide an estimate of the range of quenching rate constant. Deviation from linearity is particularly prominent at higher concentration of quencher, where permanent photochemistry is more noticeable.

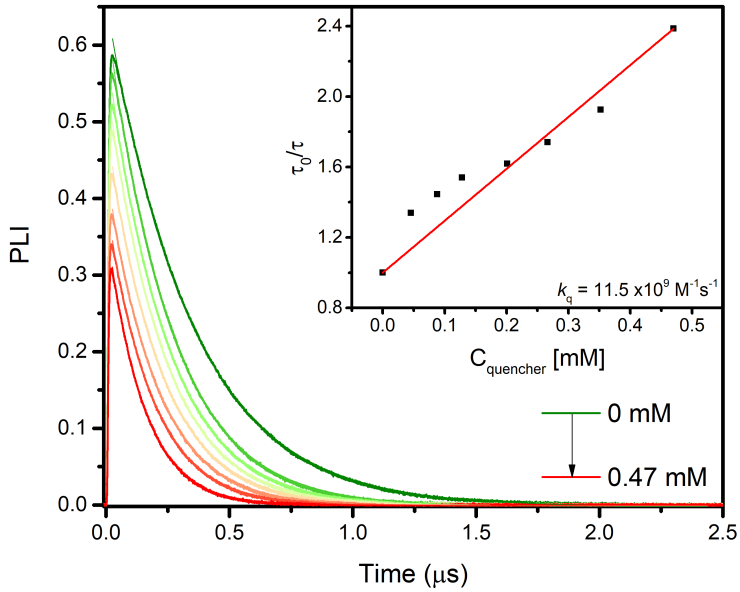

Figure S37. Excited-state quenching of [Ir(ppy)$_3$] in the presence of increasing amounts of **X$_4$-B**. Experiments were carried out in argon purged CH_3CN containing 0.1M $TBABF_4$. The inset represents the Stern-Volmer plot from which the quenching rate constant (k_q) was determined. The linear relationship does not adequately fit the data but was used to provide an estimate of the range of quenching rate constant. Deviation from linearity is particularly prominent at higher concentration of quencher, where permanent photochemistry is more noticeable.

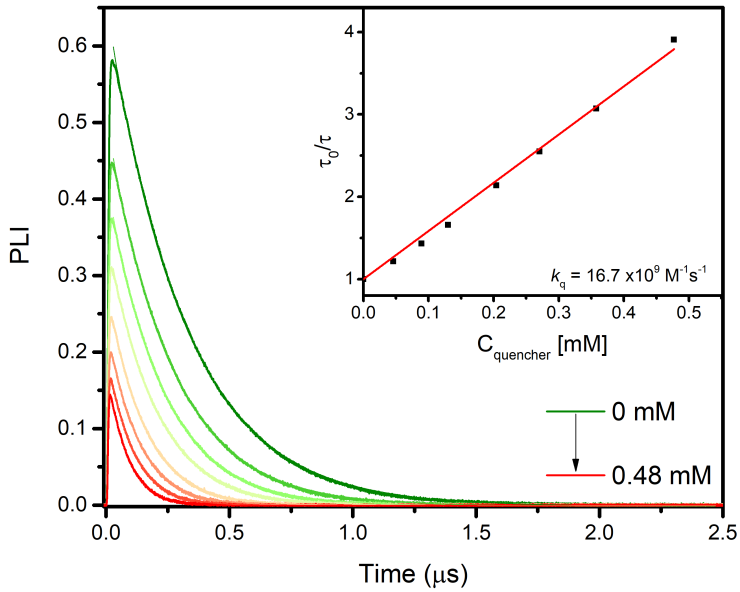

Figure S38. Excited-state quenching of [Ir(ppy)$_3$] in the presence of increasing amounts of **X$_4$-C**. Experiments were carried out in argon purged CH_3CN containing 0.1M $TBABF_4$. The inset represents the Stern-Volmer plot from which the quenching rate constant (k_q) was determined.

Stern-Volmer Experiments with $[Ir(ppy)_2(dtb)]^+$

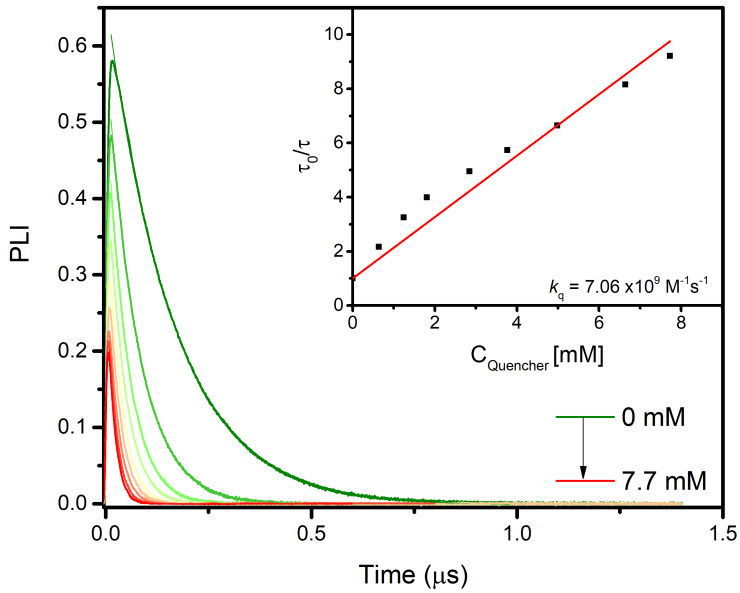

Figure S39. Excited-state quenching of $[Ir(ppy)_2(dtb)]^+$ in the presence of increasing amounts of 4-bromo-benzene-diazonium tetrafluoroborate. Experiments were carried out in argon purged CH_3CN containing 0.1M $TBABF_4$. The inset represents the Stern-Volmer plot from which the quenching rate constant (k_q) was determined.

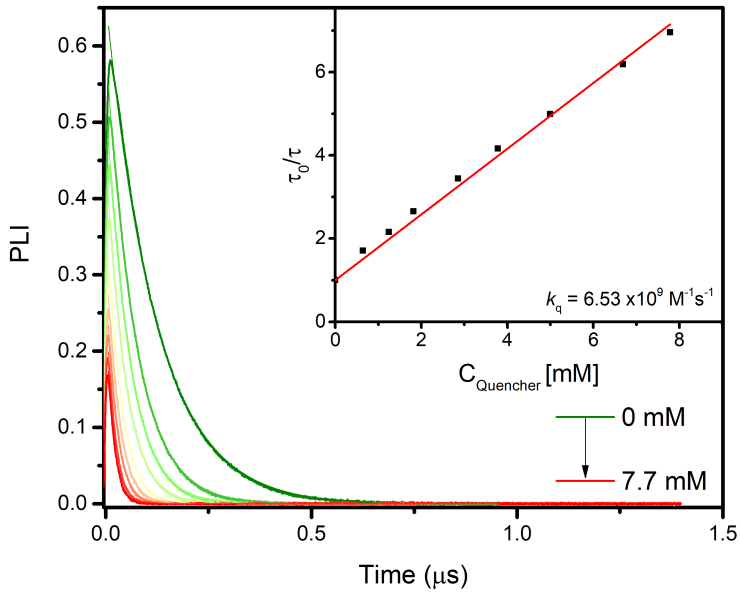

Figure S40. Excited-state quenching of $[Ir(ppy)_2(dtb)]^+$ in the presence of increasing amounts of 4-CF_3-benzene-diazonium tetrafluoroborate. Experiments were carried out in argon purged CH_3CN containing 0.1M $TBABF_4$. The inset represents the Stern-Volmer plot from which the quenching rate constant (k_q) was determined.

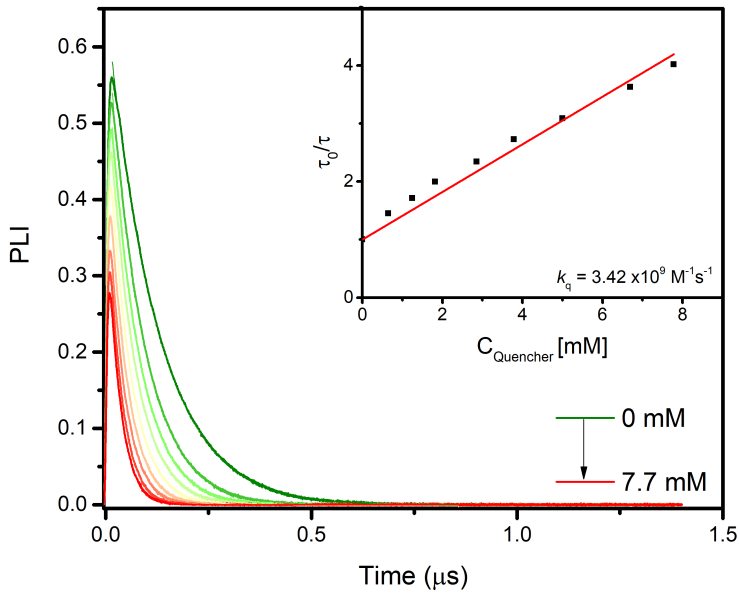

Figure S41. Excited-state quenching of $[Ir(ppy)_2(dtb)]^+$ in the presence of increasing amounts of 4-carboxylate-benzene-diazonium. Experiments were carried out in argon purged CH_3CN containing 0.1M $TBABF_4$. The inset represents the Stern-Volmer plot from which the quenching rate constant (k_q) was determined.

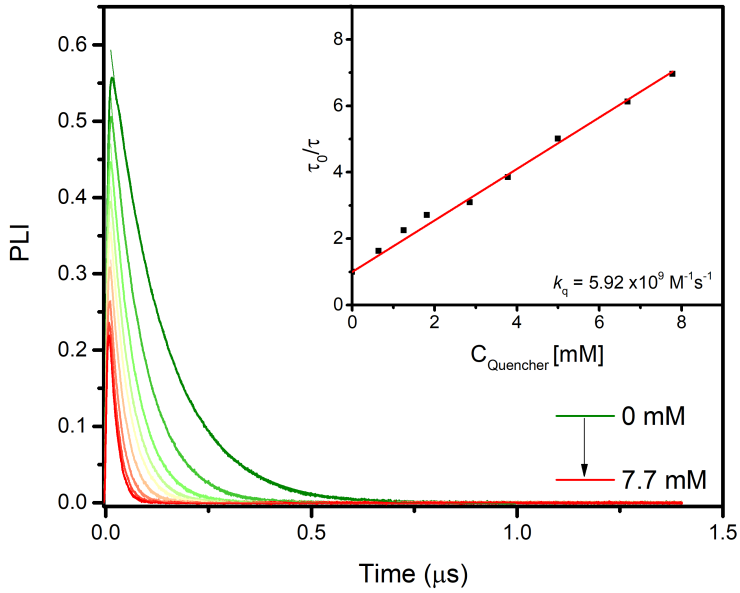

Figure S42. Excited-state quenching of $[Ir(ppy)_2(dtb)]^+$ in the presence of increasing amounts of 4-ethylester-benzene-diazonium tetrafluoroborate. Experiments were carried out in argon purged CH_3CN containing 0.1M $TBABF_4$. The inset represents the Stern-Volmer plot from which the quenching rate constant (k_q) was determined.

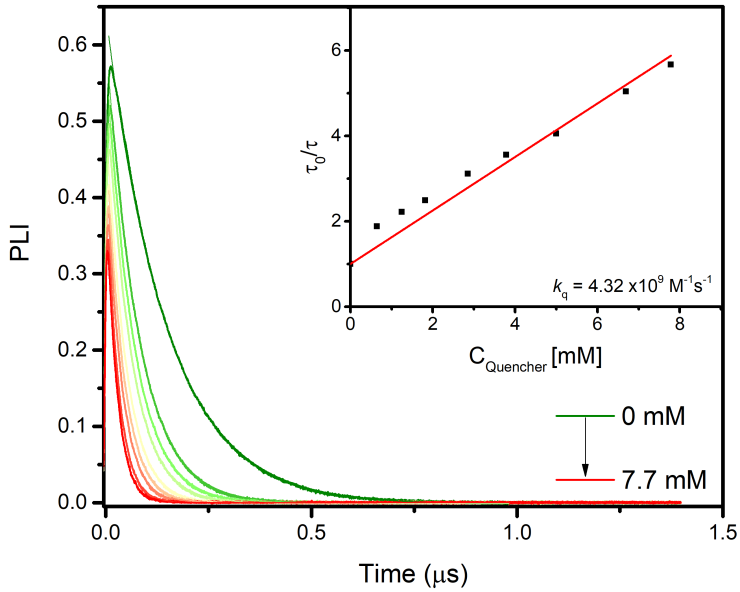

Figure S43. Excited-state quenching of $[Ir(ppy)_2(dtb)]^+$ in the presence of increasing amounts of 4-cyclohexyl-benzene-diazonium tetrafluoroborate. Experiments were carried out in argon purged CH_3CN containing 0.1M $TBABF_4$. The inset represents the Stern-Volmer plot from which the quenching rate constant (k_q) was determined.

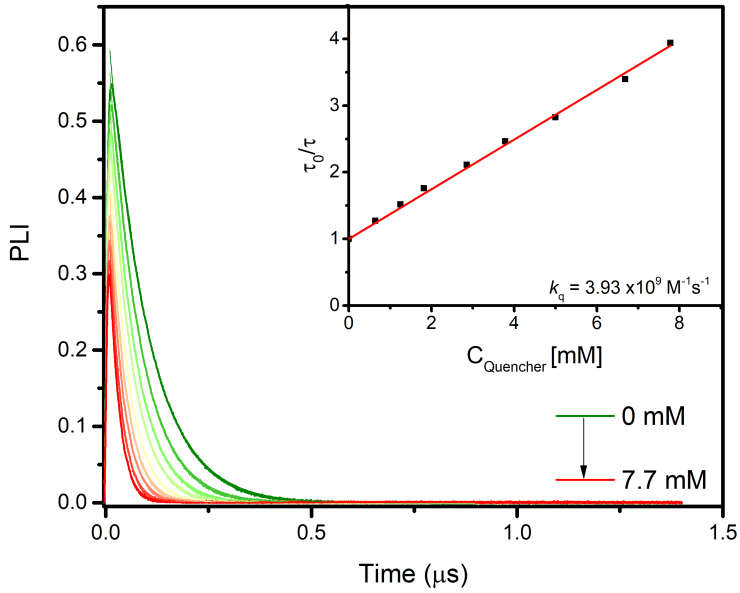

Figure S44. Excited-state quenching of $[Ir(ppy)_2(dtb)]^+$ in the presence of increasing amounts of 4-ethyl-benzene-diazonium tetrafluoroborate. Experiments were carried out in argon purged CH_3CN containing 0.1M $TBABF_4$. The inset represents the Stern-Volmer plot from which the quenching rate constant (k_q) was determined.

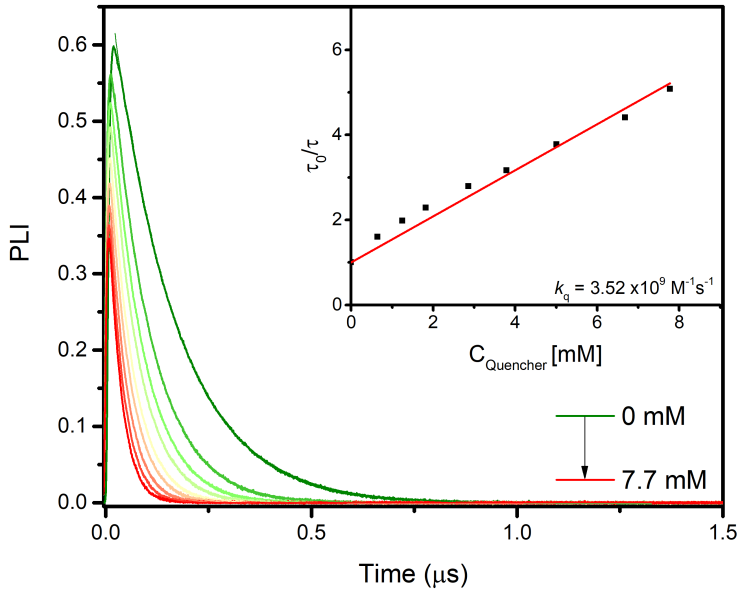

Figure S45. Excited-state quenching of $[Ir(ppy)_2(dtb)]^+$ in the presence of increasing amounts of 4-methoxy-benzene-diazonium tetrafluoroborate. Experiments were carried out in argon purged CH_3CN containing 0.1M $TBABF_4$. The inset represents the Stern-Volmer plot from which the quenching rate constant (k_q) was determined.

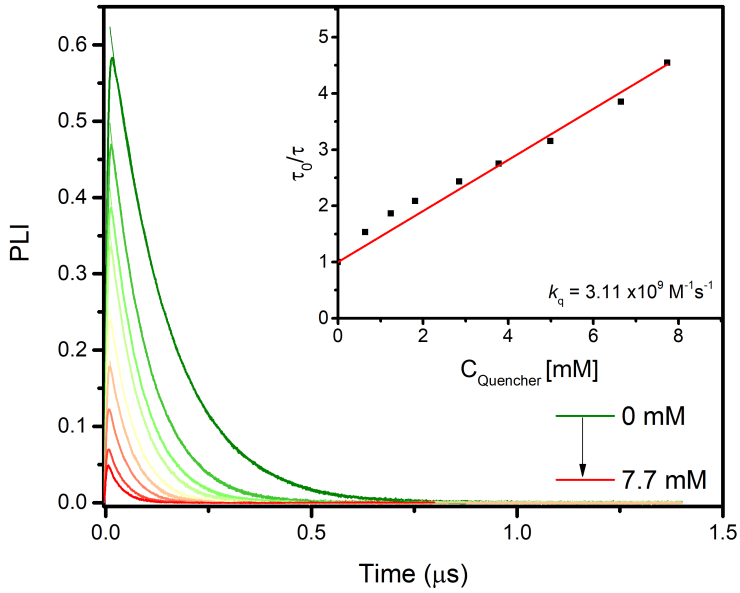

Figure S46. Excited-state quenching of $[Ir(ppy)_2(dtb)]^+$ in the presence of increasing amounts of 4-(N,N)-diethylamine-benzene-diazonium tetrafluoroborate. Experiments were carried out in argon purged CH_3CN containing 0.1M $TBABF_4$. The inset represents the Stern-Volmer plot from which the quenching rate constant (k_q) was determined.

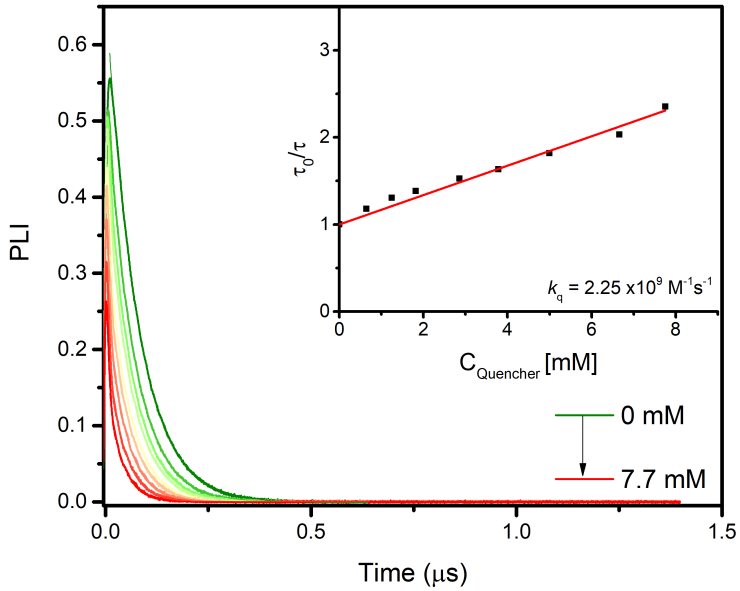

Figure S47. Excited-state quenching of $[Ir(ppy)_2(dtb)]^+$ in the presence of increasing amounts of 4-(N,N-dimethylamine-benzene-diazonium tetrafluoroborate. Experiments were carried out in argon purged CH_3CN containing 0.1M $TBABF_4$. The inset represents the Stern-Volmer plot from which the quenching rate constant (k_q) was determined.

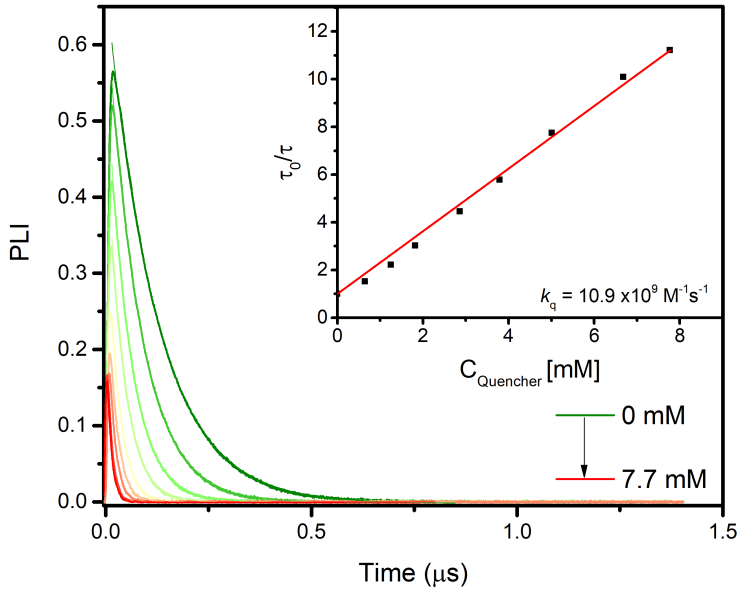

Figure S48. Excited-state quenching of $[Ir(ppy)_2(dtb)]^+$ in the presence of increasing amounts of 4-nitro-benzene-diazonium tetrafluoroborate. Experiments were carried out in argon purged CH_3CN containing 0.1M $TBABF_4$. The inset represents the Stern-Volmer plot from which the quenching rate constant (k_q) was determined.

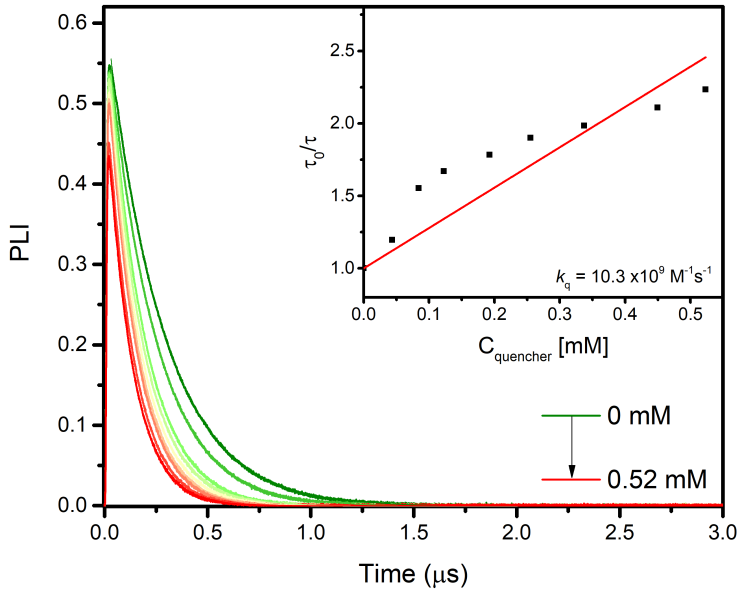

Figure S49. Excited-state quenching of $[Ir(ppy)_2(dtb)]^+$ in the presence of increasing amounts of **X_4-A**. Experiments were carried out in argon purged CH_3CN containing 0.1M $TBABF_4$. The inset represents the Stern-Volmer plot from which the quenching rate constant (k_q) was determined. The linear relationship does not adequately fit the data but was used to provide an estimate of the range of quenching rate constant. Deviation from linearity is particularly prominent at higher concentration of quencher, where permanent photochemistry is more noticeable.

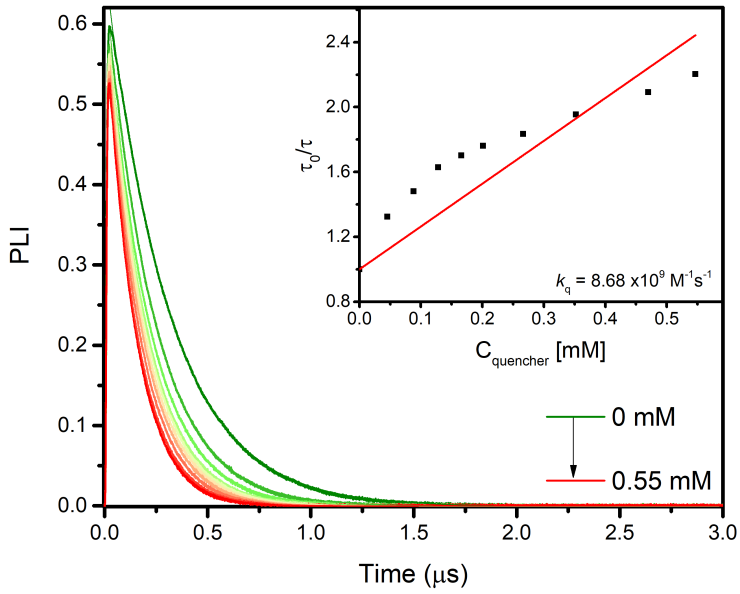

Figure S50. Excited-state quenching of $[Ir(ppy)_2(dtb)]^+$ in the presence of increasing amounts of **X_4-B**. Experiments were carried out in argon purged CH_3CN containing 0.1M $TBABF_4$. The inset represents the Stern-Volmer plot from which the quenching rate constant (k_q) was determined. The linear relationship does not adequately fit the data but was used to provide an estimate of the range of quenching rate constant. Deviation from linearity is particularly prominent at higher concentration of quencher, where permanent photochemistry is more noticeable.

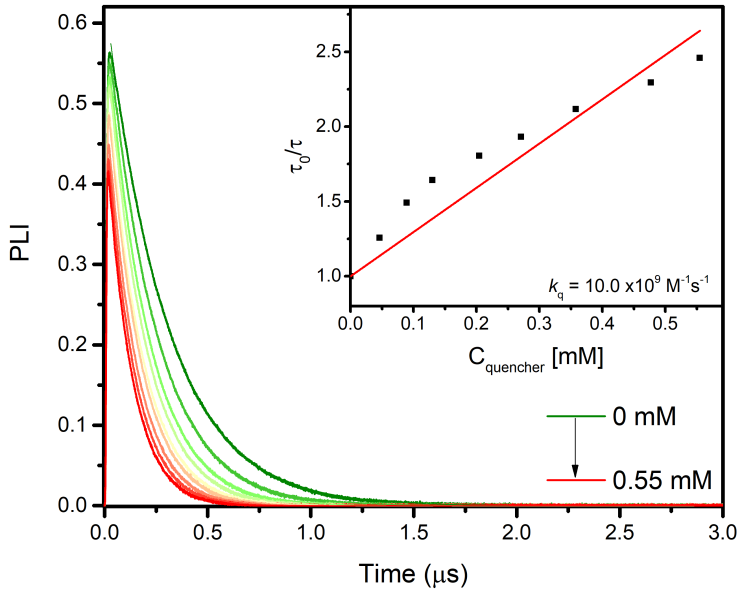

Figure S51. Excited-state quenching of $[Ir(ppy)_2(dtb)]^+$ in the presence of increasing amounts of **X_4-C**. Experiments were carried out in argon purged CH_3CN containing 0.1M $TBABF_4$. The inset represents the Stern-Volmer plot from which the quenching rate constant (k_q) was determined.

Stern-Volmer Experiments with $[Ir((dFCF_3)ppy)_2(dtb)]^+$

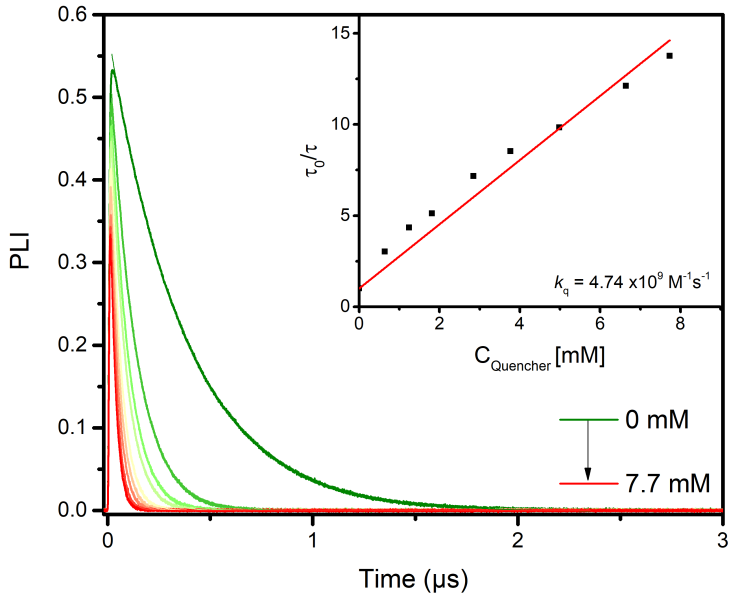

Figure S52. Excited-state quenching of $[Ir((dFCF_3)ppy)_2(dtb)]^+$ in the presence of increasing amounts of 4-bromo-benzene-diazonium tetrafluoroborate. Experiments were carried out in argon purged CH_3CN containing 0.1M $TBABF_4$. The inset represents the Stern-Volmer plot from which the quenching rate constant (k_q) was determined.

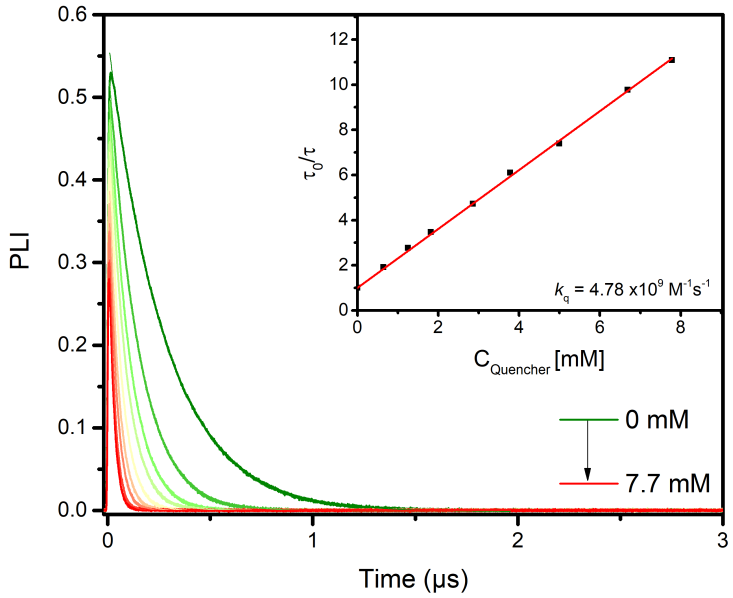

Figure S53. Excited-state quenching of $[Ir((dFCF_3)ppy)_2(dtb)]^+$ in the presence of increasing amounts of 4-CF_3-benzene-diazonium tetrafluoroborate. Experiments were carried out in argon purged CH_3CN containing 0.1M $TBABF_4$. The inset represents the Stern-Volmer plot from which the quenching rate constant (k_q) was determined.

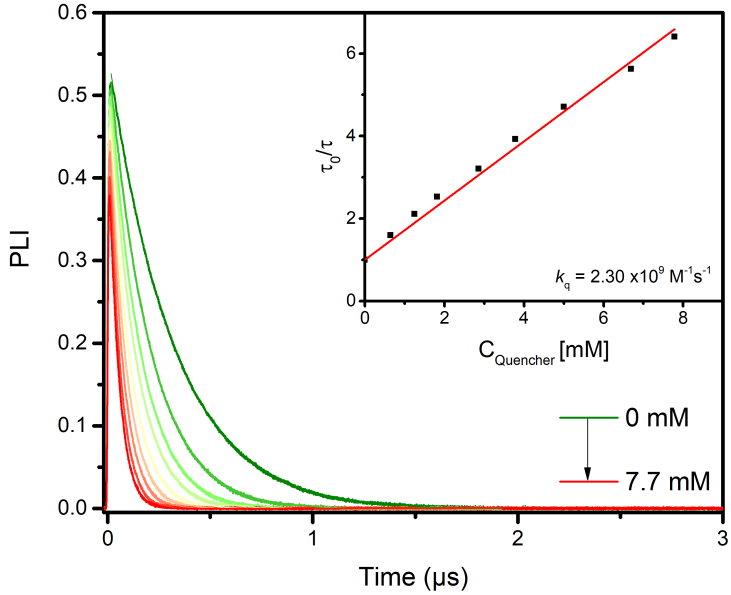

Figure S54. Excited-state quenching of $[Ir((dFCF_3)ppy)_2(dtb)]^+$ in the presence of increasing amounts of 4-carboxylate-benzene-diazonium tetrafluoroborate. Experiments were carried out in argon purged CH_3CN containing 0.1M $TBABF_4$. The inset represents the Stern-Volmer plot from which the quenching rate constant (k_q) was determined.

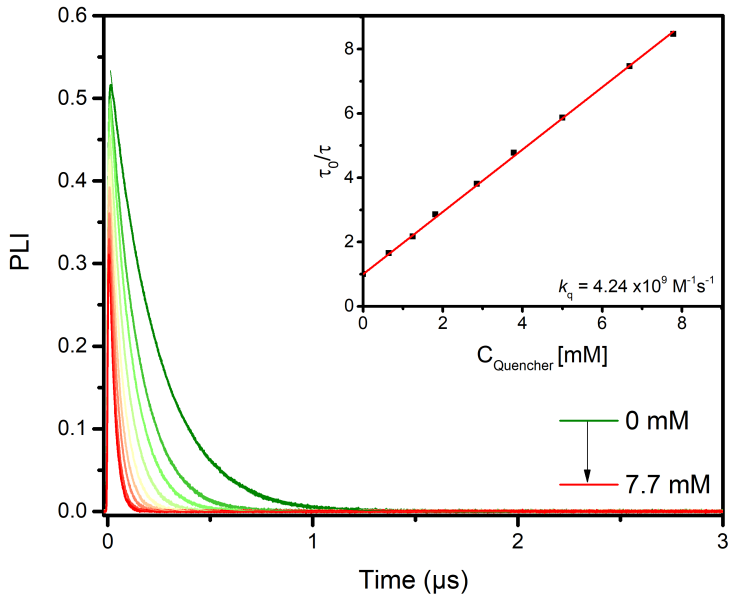

Figure S55. Excited-state quenching of $[Ir((dFCF_3)ppy)_2(dtb)]^+$ in the presence of increasing amounts of 4-ethylester-benzene-diazonium tetrafluoroborate. Experiments were carried out in argon purged CH_3CN containing 0.1M $TBABF_4$. The inset represents the Stern-Volmer plot from which the quenching rate constant (k_q) was determined.

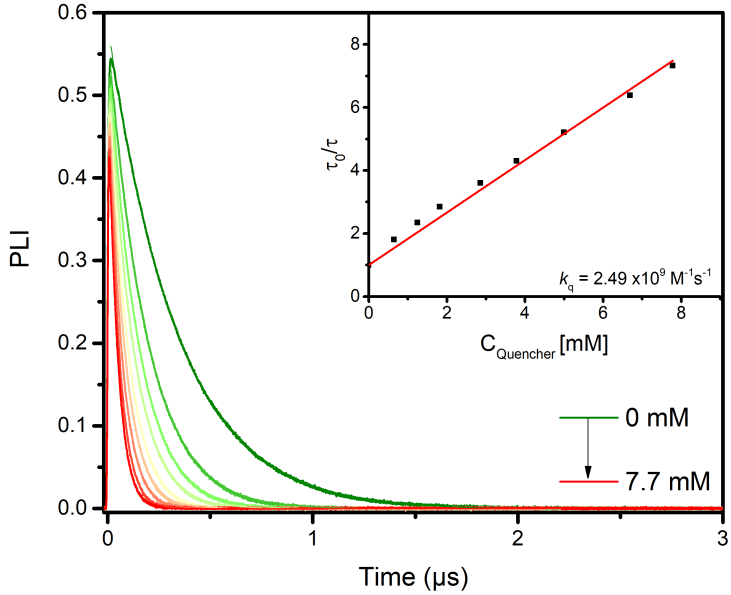

Figure S56. Excited-state quenching of $[Ir((dFCF_3)ppy)_2(dtb)]^+$ in the presence of increasing amounts of 4-cyclohexyl-benzene-diazonium tetrafluoroborate. Experiments were carried out in argon purged CH_3CN containing 0.1M $TBABF_4$. The inset represents the Stern-Volmer plot from which the quenching rate constant (k_q) was determined.

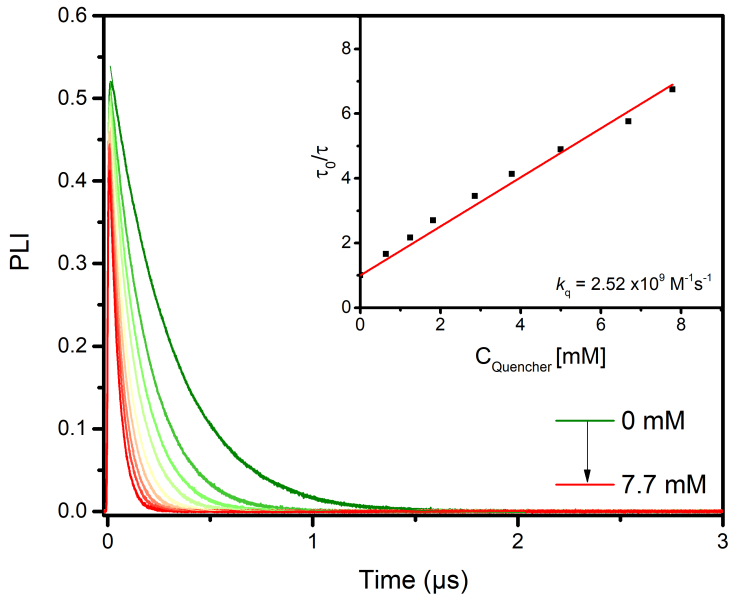

Figure S57. Excited-state quenching of $[Ir((dFCF_3)ppy)_2(dtb)]^+$ in the presence of increasing amounts of 4-ethyl-benzene-diazonium tetrafluoroborate. Experiments were carried out in argon purged CH_3CN containing 0.1M $TBABF_4$. The inset represents the Stern-Volmer plot from which the quenching rate constant (k_q) was determined.

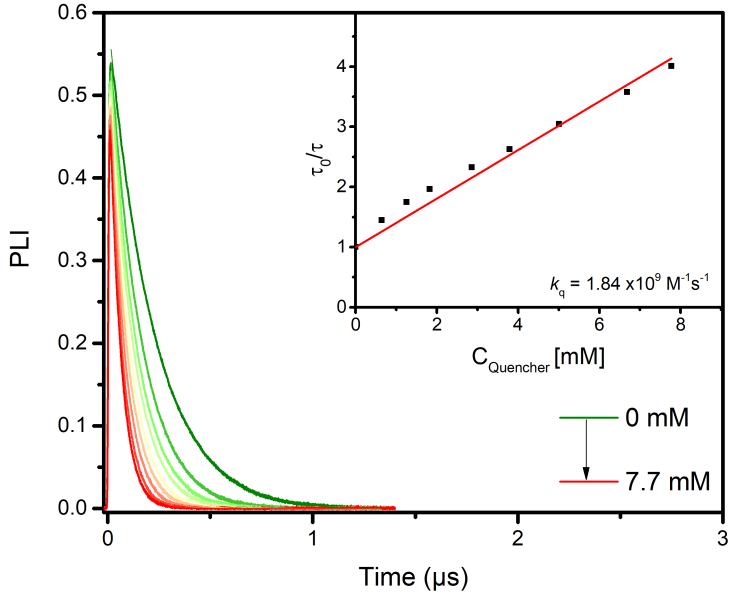

Figure S58. Excited-state quenching of $[Ir((dFCF_3)ppy)_2(dtb)]^+$ in the presence of increasing amounts of 4-methoxy-benzene-diazonium tetrafluoroborate. Experiments were carried out in argon purged CH_3CN containing 0.1M $TBABF_4$. The inset represents the Stern-Volmer plot from which the quenching rate constant (k_q) was determined.

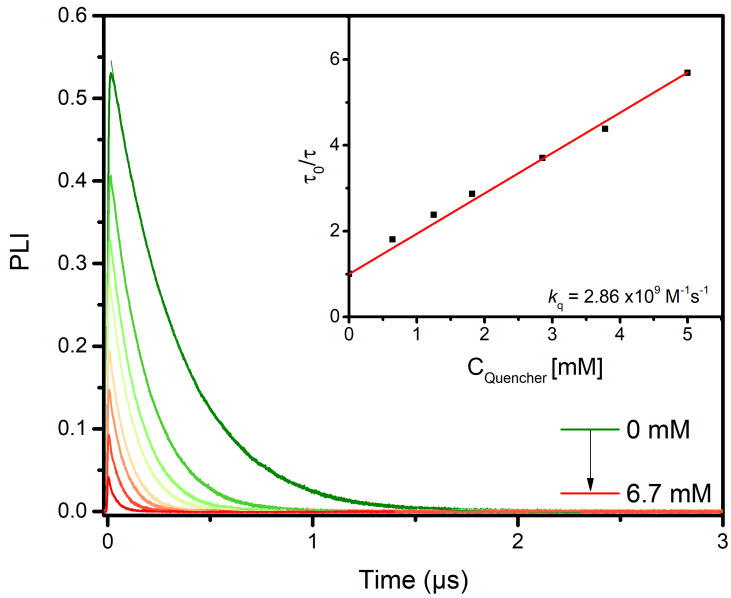

Figure S59. Excited-state quenching of $[Ir((dFCF_3)ppy)_2(dtb)]^+$ in the presence of increasing amounts of 4-(N,N)-diethylamine-benzene-diazonium tetrafluoroborate. Experiments were carried out in argon purged CH_3CN containing 0.1M $TBABF_4$. The inset represents the Stern-Volmer plot from which the quenching rate constant (k_q) was determined.

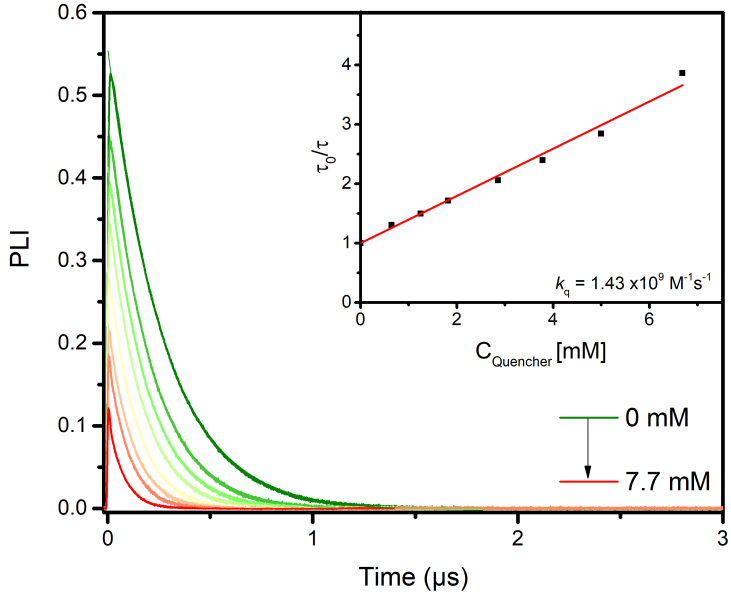

Figure S60. Excited-state quenching of $[Ir((dFCF_3)ppy)_2(dtb)]^+$ in the presence of increasing amounts of 4-(N,N)-dimethylamine-benzene-diazonium tetrafluoroborate. Experiments were carried out in argon purged CH_3CN containing 0.1M $TBABF_4$. The inset represents the Stern-Volmer plot from which the quenching rate constant (k_q) was determined.

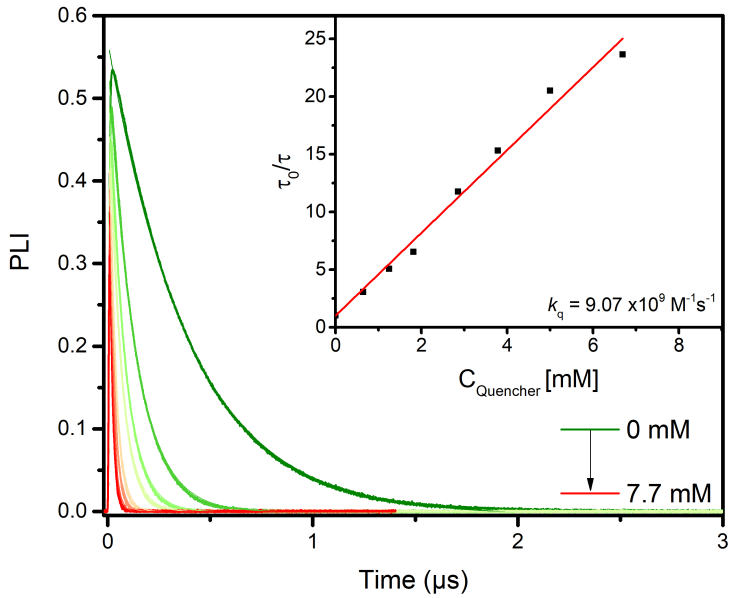

Figure S61. Excited-state quenching of $[Ir((dFCF_3)ppy)_2(dtb)]^+$ in the presence of increasing amounts of 4-nitro-benzene-diazonium tetrafluoroborate. Experiments were carried out in argon purged CH_3CN containing 0.1M $TBABF_4$. The inset represents the Stern-Volmer plot from which the quenching rate constant (k_q) was determined.

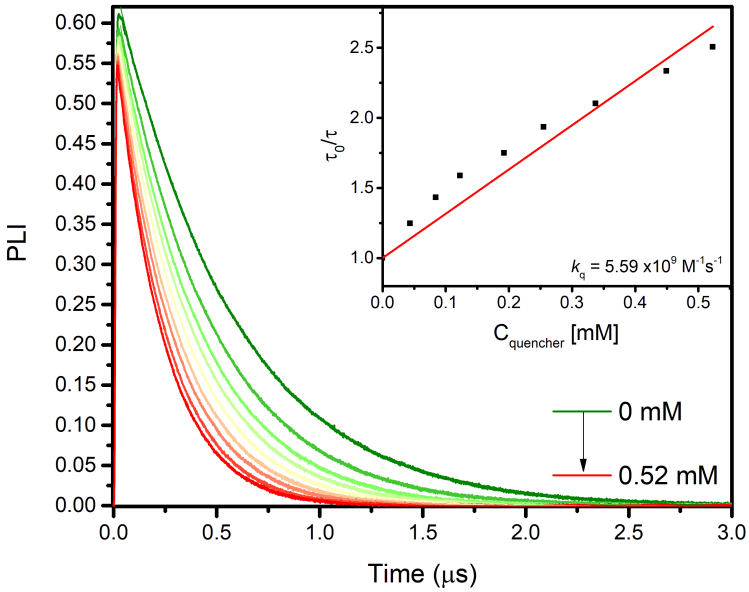

Figure S62. Excited-state quenching of $[Ir((dFCF_3)ppy)_2(dtb)]^+$ in the presence of increasing amounts of **X₄-A**. Experiments were carried out in argon purged CH_3CN containing 0.1M $TBABF_4$. The inset represents the Stern-Volmer plot from which the quenching rate constant (k_q) was determined.

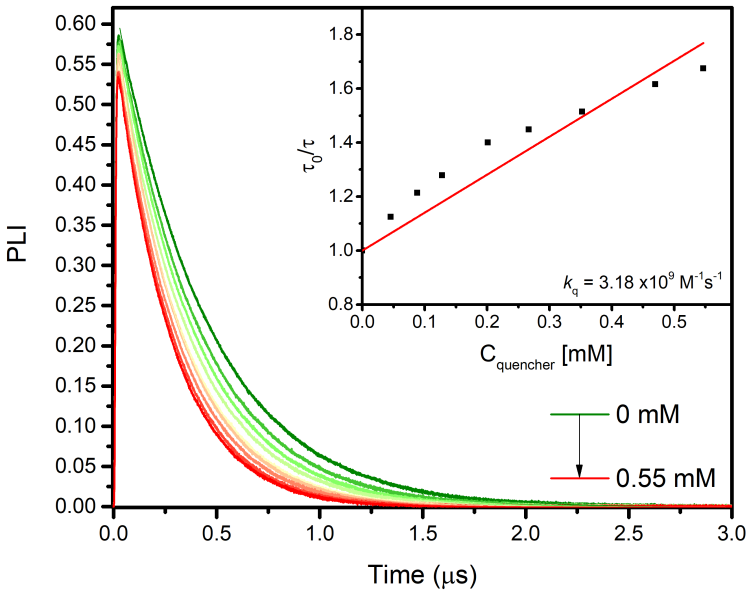

Figure S63. Excited-state quenching of $[Ir((dFCF_3)ppy)_2(dtb)]^+$ in the presence of increasing amounts of **X₄-B**. Experiments were carried out in argon purged CH_3CN containing 0.1M $TBABF_4$. The inset represents the Stern-Volmer plot from which the quenching rate constant (k_q) was determined.

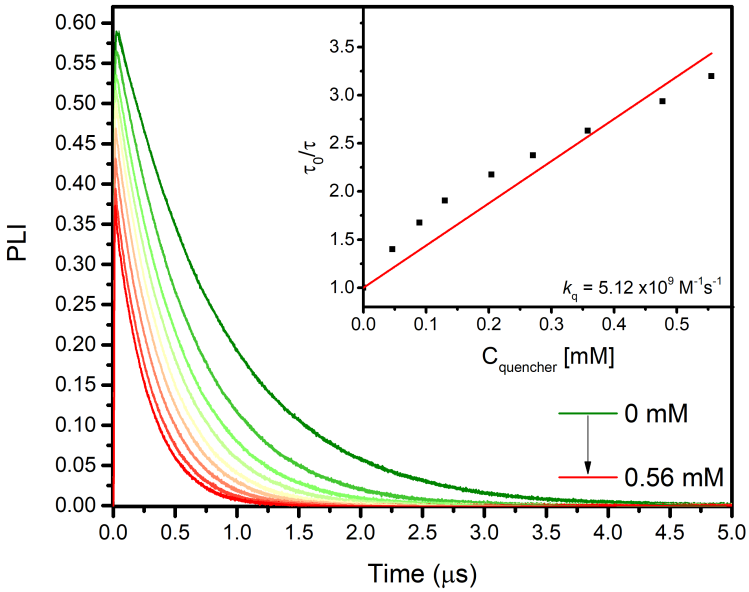

Figure S64. Excited-state quenching of $[Ir((dFCF_3)ppy)_2(dtb)]^+$ in the presence of increasing amounts of **X_4-C**. Experiments were carried out in argon purged CH_3CN containing 0.1M $TBABF_4$. The inset represents the Stern-Volmer plot from which the quenching rate constant (k_q) was determined.

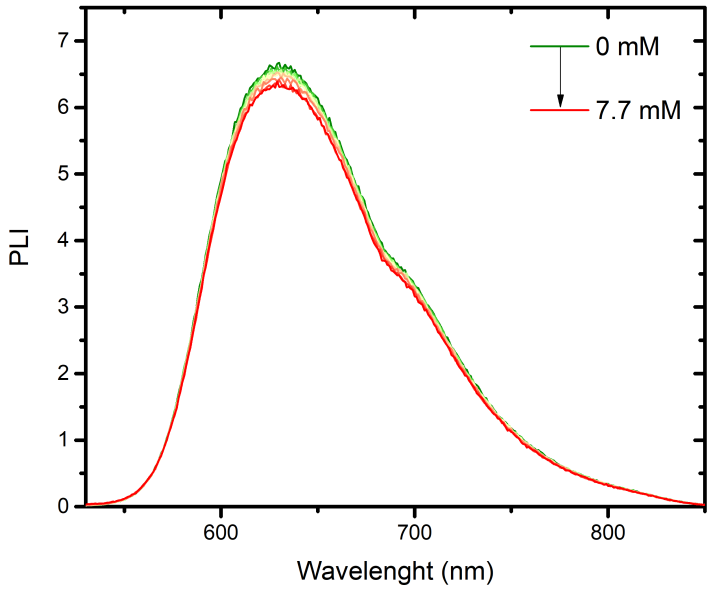

Figure S65. Excited-state quenching of $[Fe(phtmeimb)_2]^+$ in the presence of increasing amounts of 4-nitro-benzene-diazonium tetrafluoroborate. Experiments were carried out in argon purged CH_3CN containing 0.1M $TBABF_4$.

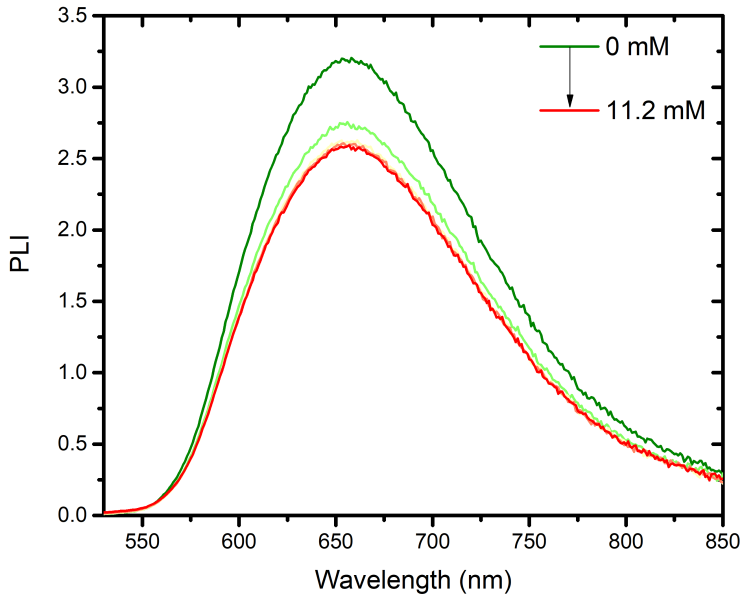

Figure S66. Excited-state quenching of $[Fe(Br\text{-}phtmeimb)_2]^+$ in the presence of increasing amounts of 4-nitro-benzene-diazonium tetrafluoroborate. Experiments were carried out in argon purged CH_3CN containing 0.1M $TBABF_4$.

Nanosecond Transient Absorption Spectroscopy

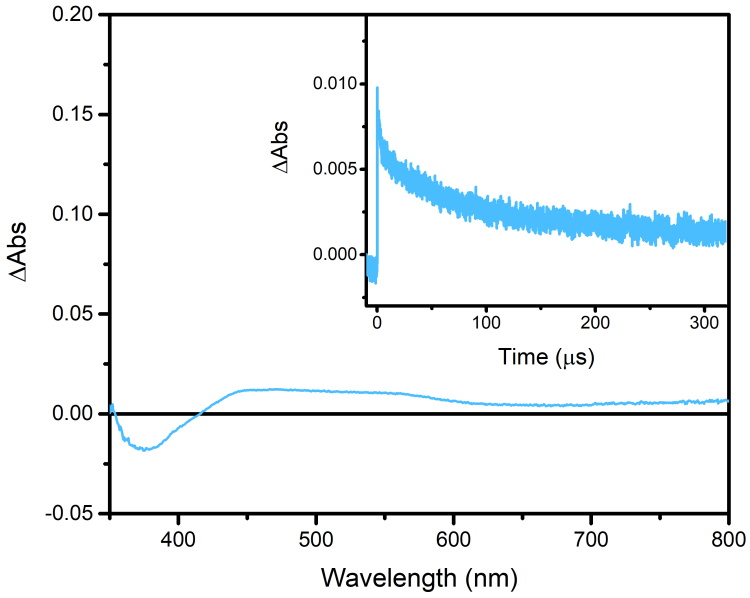

Figure S67. Nanosecond transient absorption of $[Ir((dFCF_3)ppy)_2(dtb)]^+$ recorded 100 ns (integration for 100 ns) after pulsed 420 nm light excitation (10 mJ/pulse) in the presence of 30 mM of 4-methoxy-benzene-diazonium tetrafluoroborate in argon purged acetonitrile. The inset represents transient absorption changes for the same solution recorded at 450 nm.

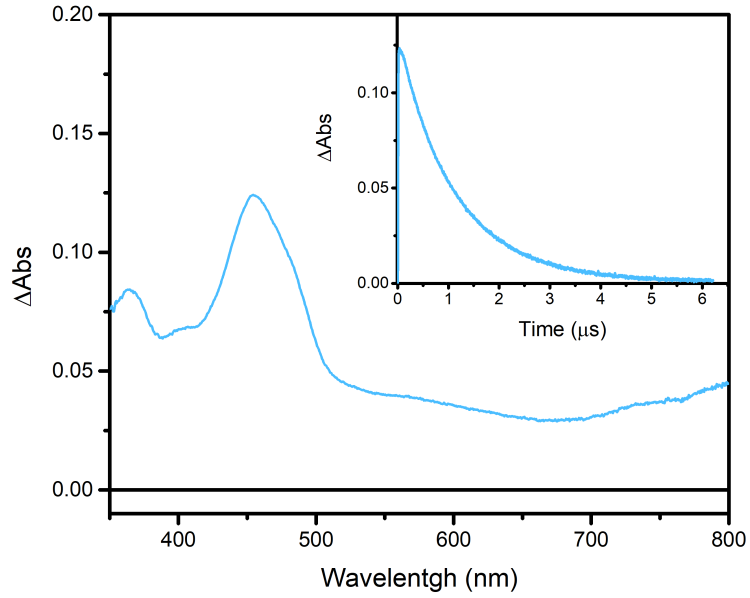

Figure S68. Nanosecond transient absorption of $[Ir((dFCF_3)ppy)_2(dtb)]^+$ recorded 10 ns (integration for 50 ns) after pulsed 420 nm light excitation (10 mJ/pulse) in argon purged acetonitrile. The inset represents transient absorption changes for the same solution recorded at 450 nm.

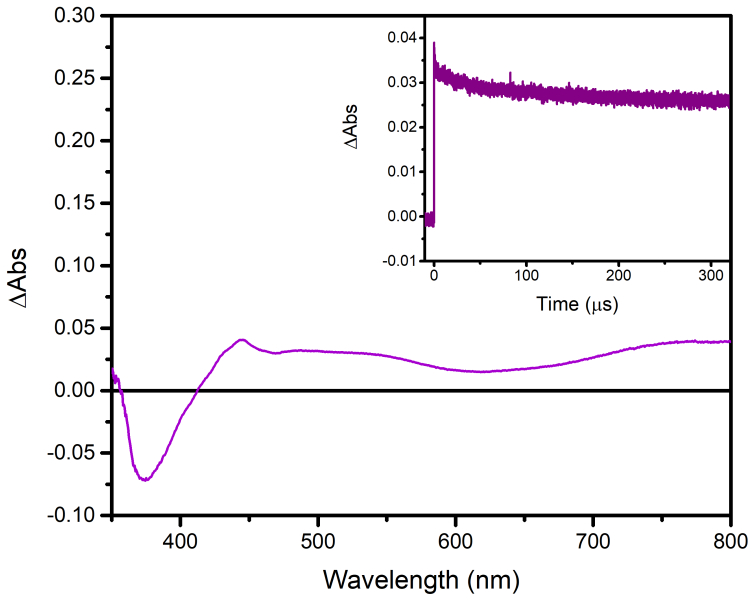

Figure S69. Nanosecond transient absorption of $[Ir(ppy)_2(dtb)]^+$ recorded 100 ns (integration for 100 ns) after pulsed 420 nm light excitation (10 mJ/pulse) in the presence of 30 mM of 4-methoxy-benzene-diazonium tetrafluoroborate in argon purged acetonitrile. The inset represents transient absorption changes for the same solution recorded at 450 nm.

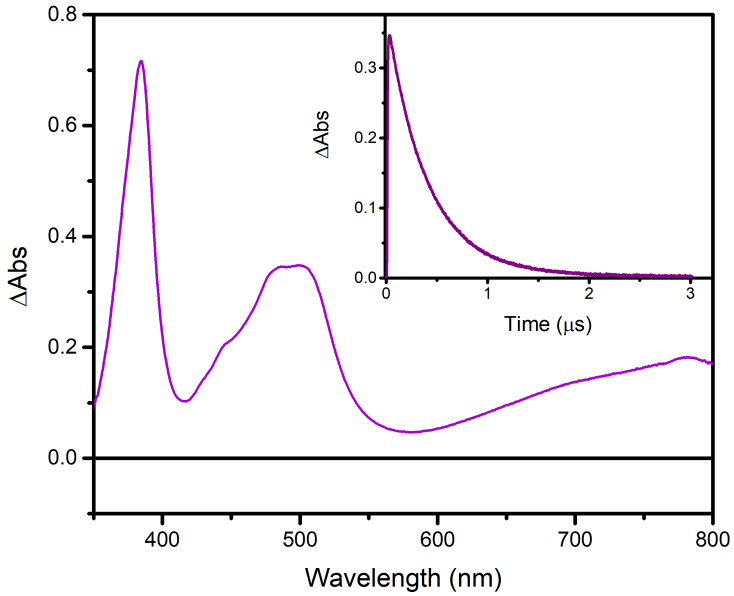

Figure S70. Nanosecond transient absorption of $[Ir(ppy)_2(dtb)]^+$ recorded 10 ns (integration for 50 ns) after pulsed 420 nm light excitation (10 mJ/pulse) in argon purged acetonitrile. The inset represents transient absorption changes for the same solution recorded at 450 nm.

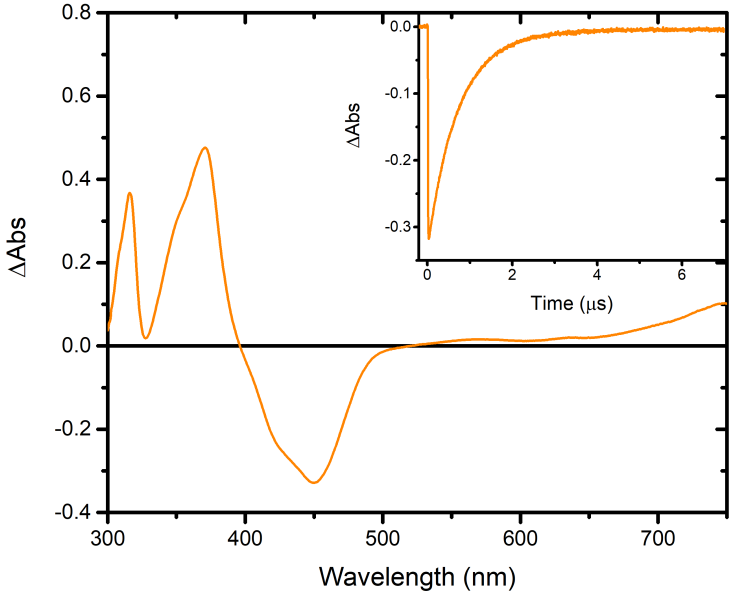

Figure S71. Nanosecond transient absorption of $[Ru(bpy)_3]^{2+}$ recorded 10 ns (integration for 50 ns) after pulsed 420 nm light excitation (10 mJ/pulse) in argon purged acetonitrile. The inset represents transient absorption changes for the same solution recorded at 450 nm.

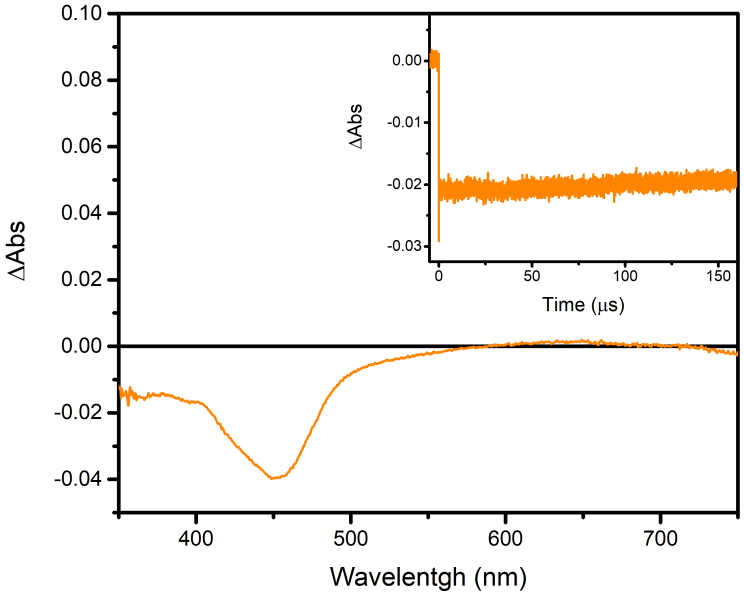

Figure S72. Nanosecond transient absorption of $[Ru(bpy)_3]^{2+}$ recorded 100 ns (integration for 100 ns) after pulsed 420 nm light excitation (10 mJ/pulse) in the presence of 30 mM of 4-methoxy-benzene-diazonium tetrafluoroborate in argon purged acetonitrile. The inset represents transient absorption changes for the same solution recorded at 450 nm.

Photostability

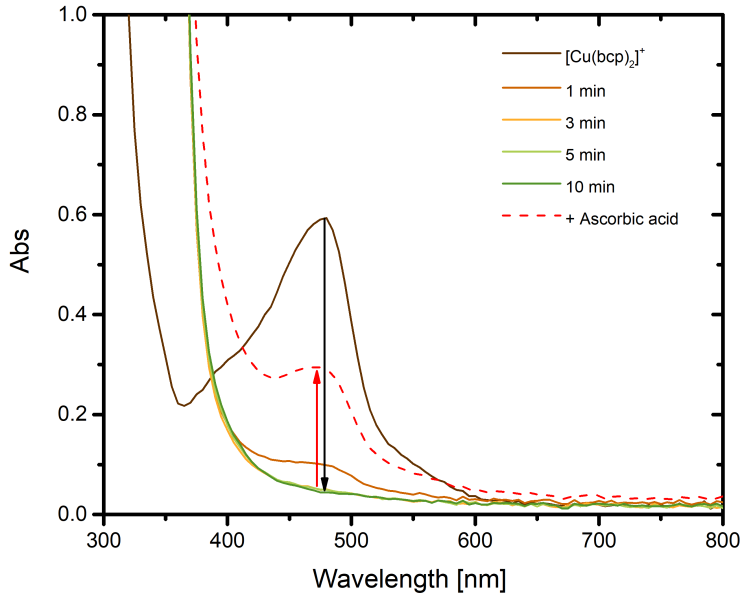

Figure S73. Photolysis experiments of $[Cu(bcp)_2]^+$ in argon purged acetonitrile in the presence of 30 mM of 4-methoxy-benzene-diazonium tetrafluoroborate. Reversibility was assessed through the addition of ascorbic acid at the end of the photolysis experiment (red dashed lines).

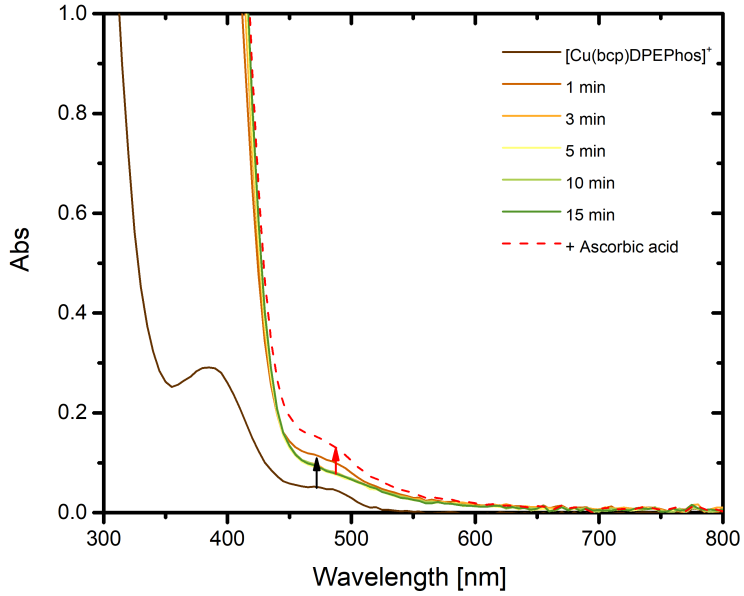

Figure S74. Photolysis experiments of $[Cu(bcp)(DPEPhos)]^+$ in argon purged acetonitrile in the presence of 30 mM of 4-methoxy-benzene-diazonium tetrafluoroborate. Reversibility was assessed through the addition of ascorbic acid at the end of the photolysis experiment (red dashed lines).

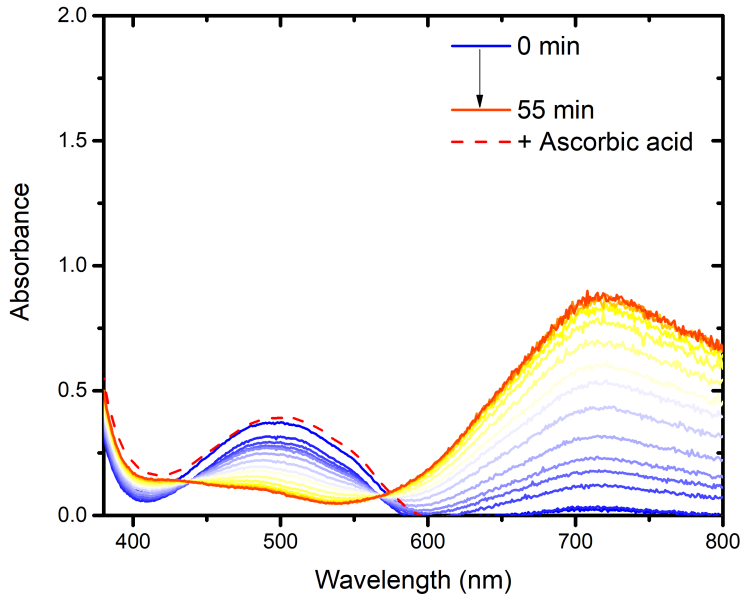

Figure S75. Photolysis experiments of $[Fe(Br\text{-}phtmeimb)_2]^+$ in argon purged acetonitrile in the presence of 30 mM of 4-methoxy-benzene-diazonium tetrafluoroborate. Reversibility was assessed through the addition of ascorbic acid at the end of the photolysis experiment (red dashed lines).

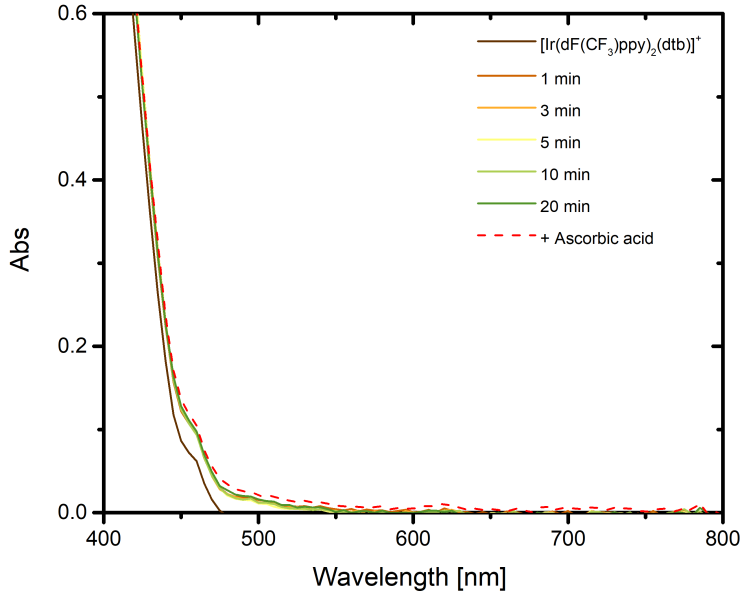

Figure S76. Photolysis experiments of $[Ir((dFCF_3)ppy)_2(dtb)]^+$ in argon purged acetonitrile in the presence of 30 mM of 4-methoxy-benzene-diazonium tetrafluoroborate. Reversibility was assessed through the addition of ascorbic acid at the end of the photolysis experiment (red dashed lines).

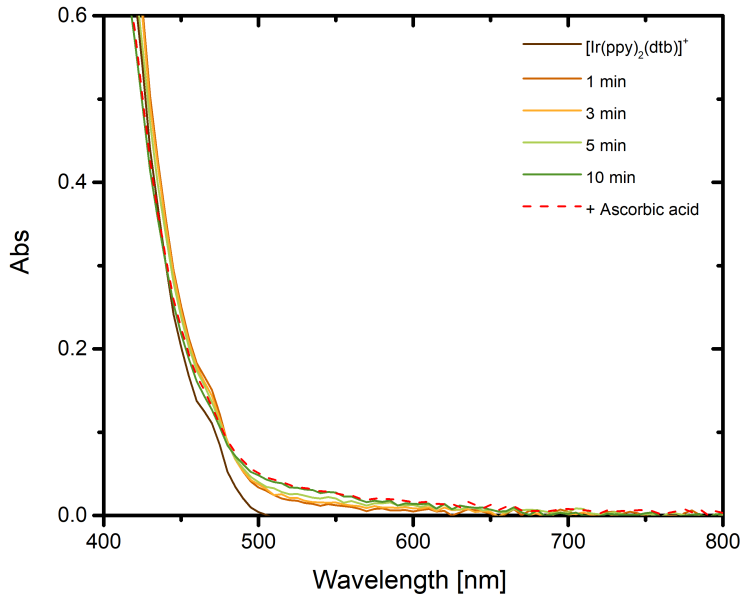

Figure S77. Photolysis experiments of $[Ir(ppy)_2(dtb)]^+$ in argon purged acetonitrile in the presence of 30 mM of 4-methoxy-benzene-diazonium tetrafluoroborate. Reversibility was assessed through the addition of ascorbic acid at the end of the photolysis experiment (red dashed lines).

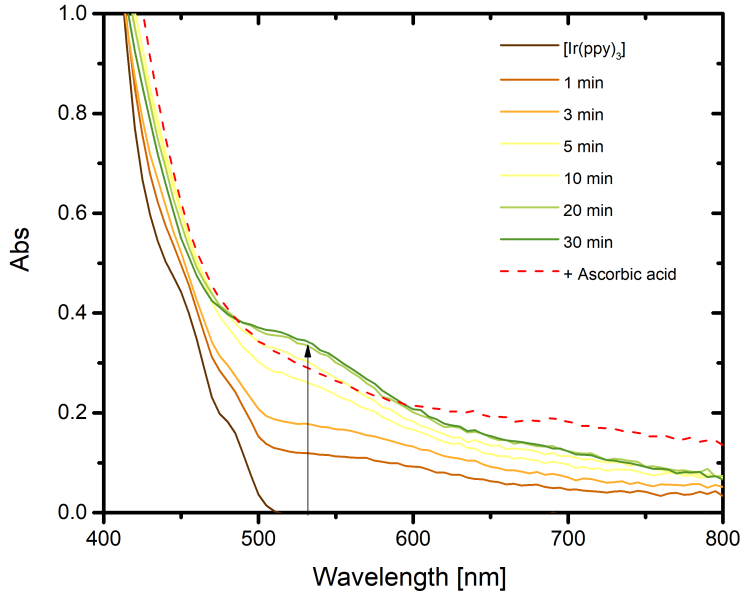

Figure S78. Photolysis experiments of $[Ir(ppy)_3]^+$ in argon purged acetonitrile in the presence of 30 mM of 4-methoxy-benzene-diazonium tetrafluoroborate. Reversibility was assessed through the addition of ascorbic acid at the end of the photolysis experiment (red dashed lines).

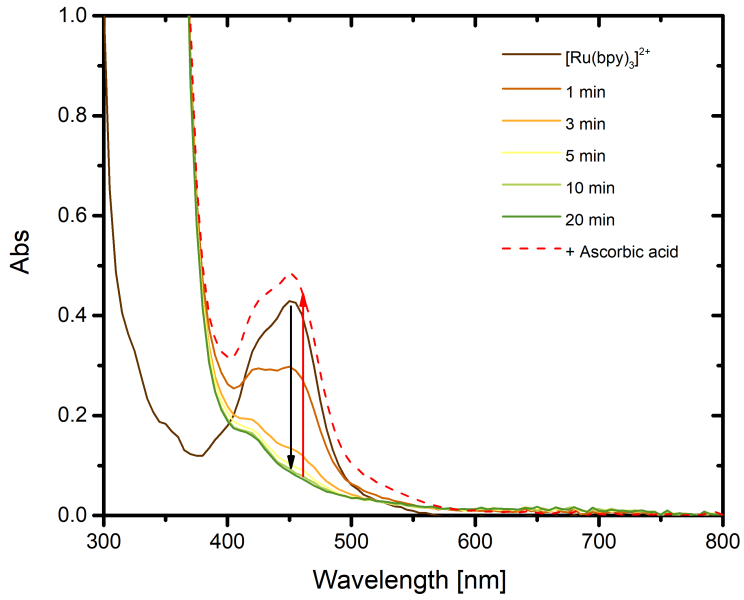

Figure S79. Photolysis experiments of $[Ru(bpy)_3]^{2+}$ in argon purged acetonitrile in the presence of 30 mM of 4-methoxy-benzene-diazonium tetrafluoroborate. Reversibility was assessed through the addition of ascorbic acid at the end of the photolysis experiment (red dashed lines).

LED Profile

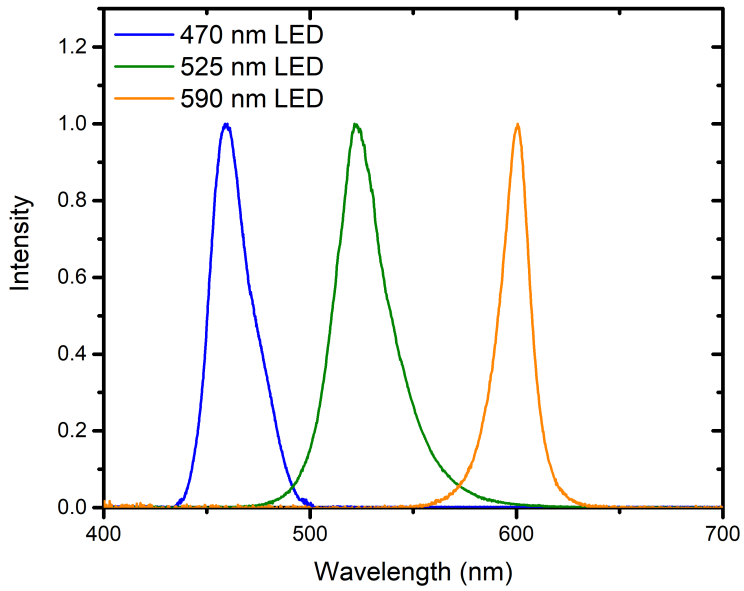

Figure S80. LED emission profile used in the present study.

Excited-State Lifetime

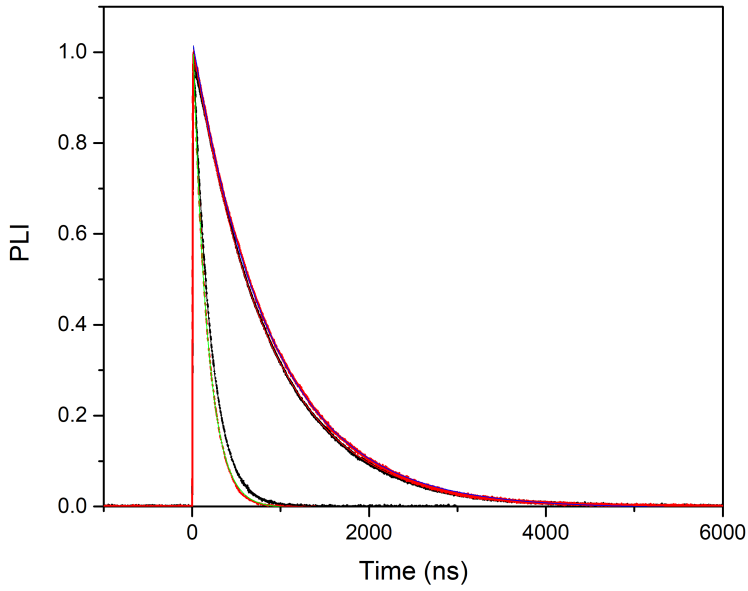

Figure S81. Excited-state lifetime of $[Ru(bpy)_3]^{2+}$ recorded in acetonitrile (Black) and acetonitrile containing 0.1M $TBABF_4$ (red) under argon (solid) and under air (dashed).

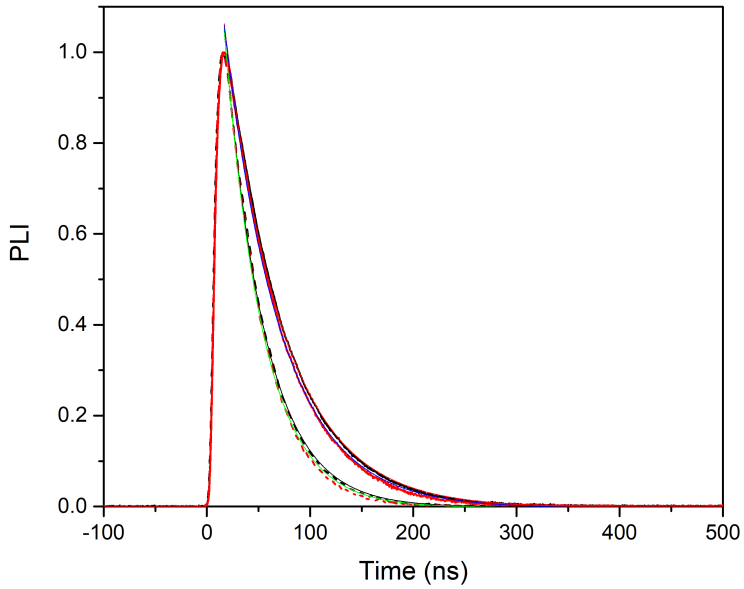

Figure S82. Excited-state lifetime of $[Os(bpy)_3]^{2+}$ recorded in acetonitrile (Black) and acetonitrile containing 0.1M $TBABF_4$ (red) under argon (solid) and under air (dashed).

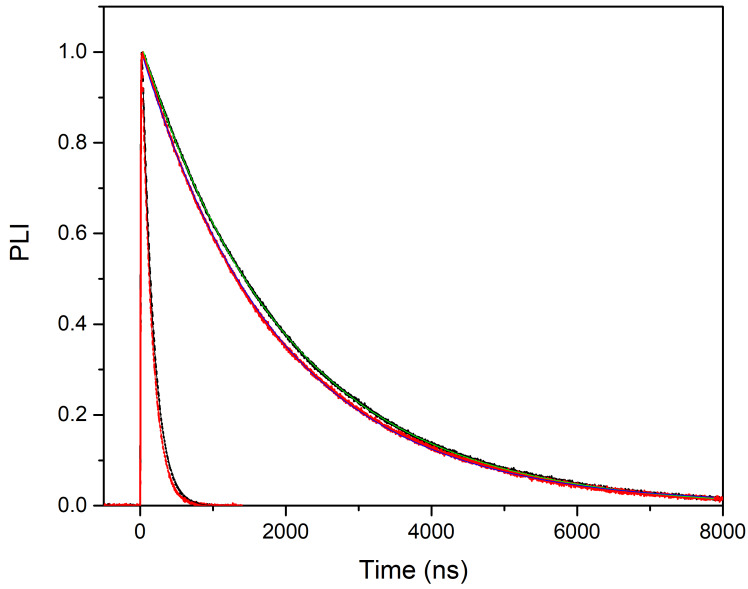

Figure S83. Excited-state lifetime of $[Ir(dF(CF_3)ppy)_2(dtb)]^+$ recorded in acetonitrile (Black) and acetonitrile containing 0.1M $TBABF_4$ (red) under argon (solid) and under air (dashed).

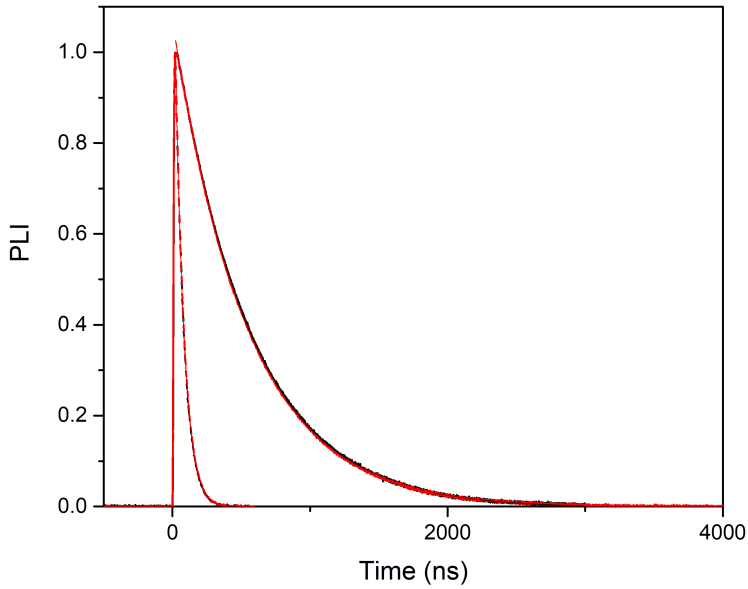

Figure S84. Excited-state lifetime of $[Ir(ppy)_2(dtb)]^+$ recorded in acetonitrile (Black) and acetonitrile containing 0.1M $TBABF_4$ (red) under argon (solid) and under air (dashed).

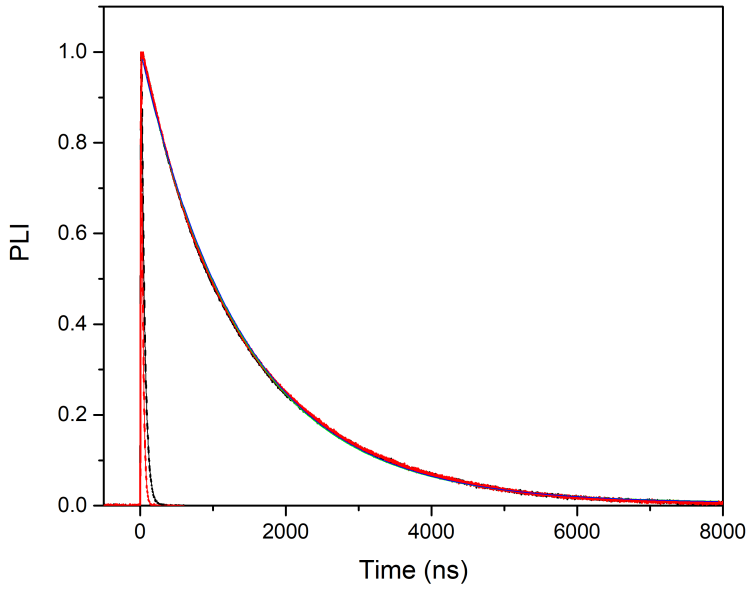

Figure S85. Excited-state lifetime of $[Ir(ppy)_3]$ recorded in acetonitrile (Black) and acetonitrile containing 0.1M $TBABF_4$ (red) under argon (solid) and under air (dashed).

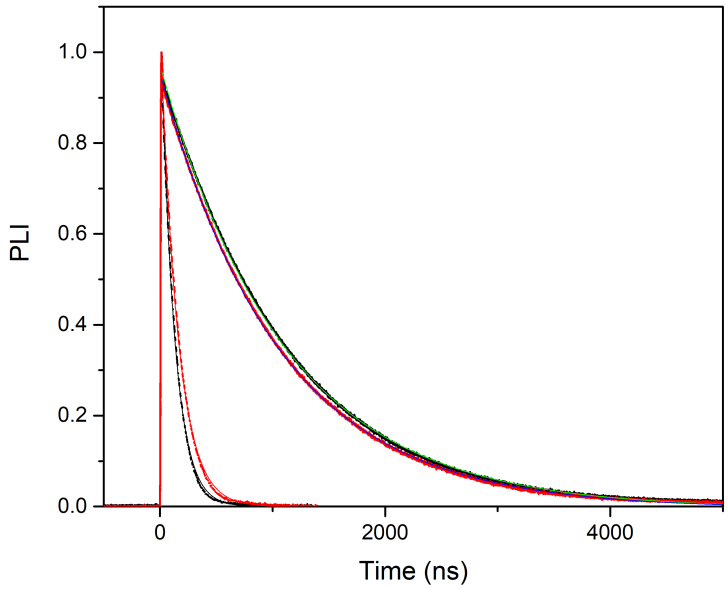

Figure S86. Excited-state lifetime of $[Cu(bcp)(DPEPhos)]^+$ recorded in acetonitrile (Black) and acetonitrile containing 0.1M $TBABF_4$ (red) under argon (solid) and under air (dashed).

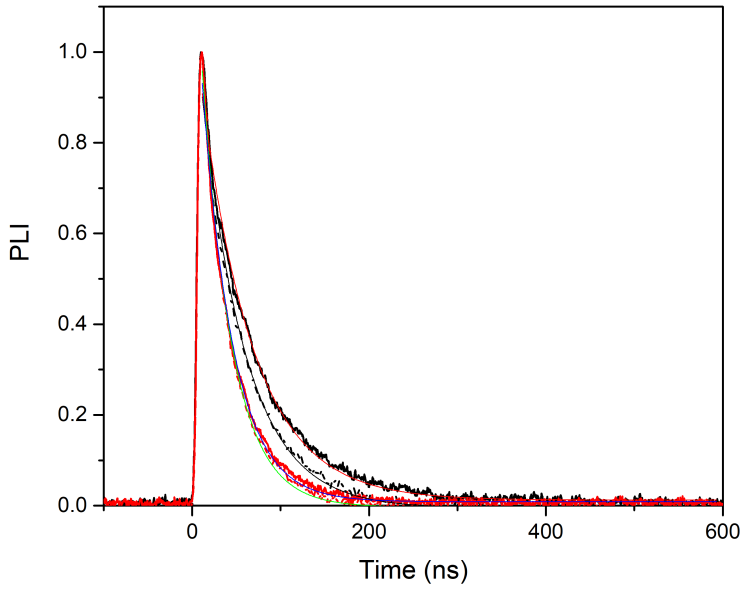

Figure S87. Excited-state lifetime of $[Cu(bcp)_2]^+$ recorded in acetonitrile (Black) and acetonitrile containing 0.1M $TBABF_4$ (red) under argon (solid) and under air (dashed).

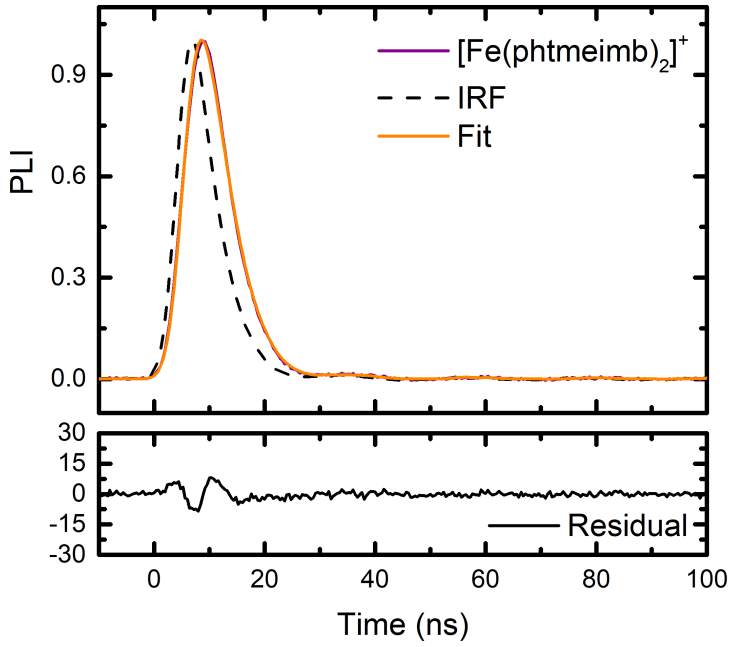

Figure S88. Reconvolution fitting used to fit the time-resolved PL data or $[Fe(phtmeimb)_2]^+$ recorded in argon-purged acetonitrile. The bottom plot shows the residual of this fit.

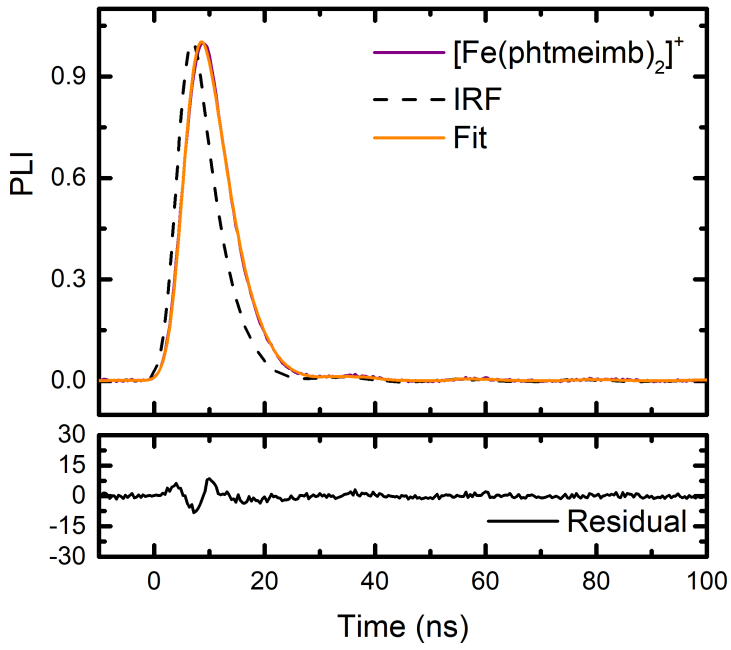

Figure S89. Reconvolution fitting used to fit the time-resolved PL data or $[Fe(phtmeimb)_2]^+$ recorded in air-equilibrated acetonitrile. The bottom plot shows the residual of this fit.

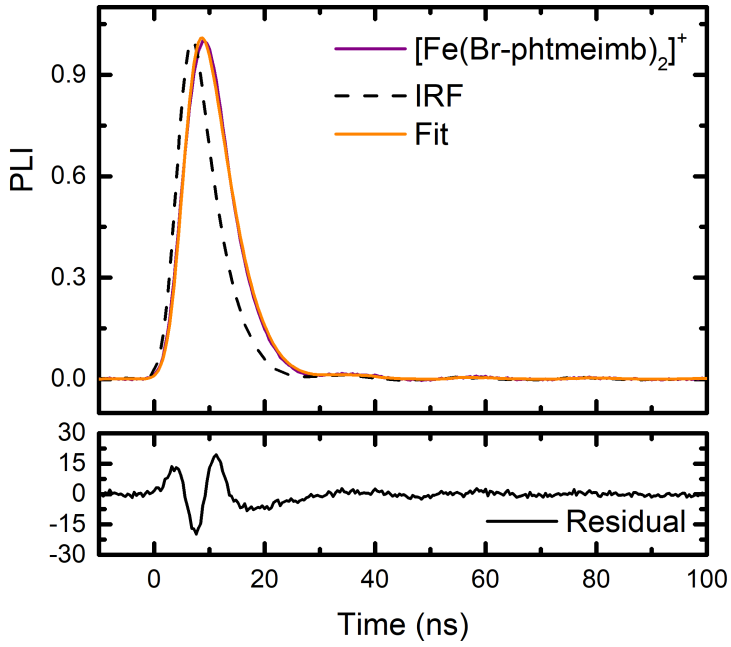

Figure S90. Reconvolution fitting used to fit the time-resolved PL data or $[Fe(Br\text{-}phtmeimb)_2]^+$ recorded in argon-purged acetonitrile. The bottom plot shows the residual of this fit.

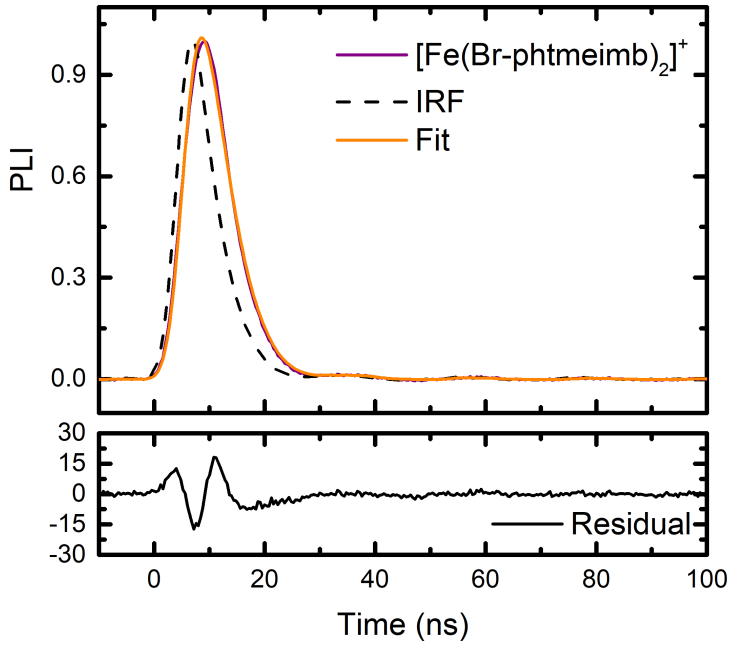

Figure S91. Reconvolution fitting used to fit the time-resolved PL data or $[Fe(Br\text{-}phtmeimb)_2]^+$ recorded in air-equilibrated acetonitrile. The bottom plot shows the residual of this fit.

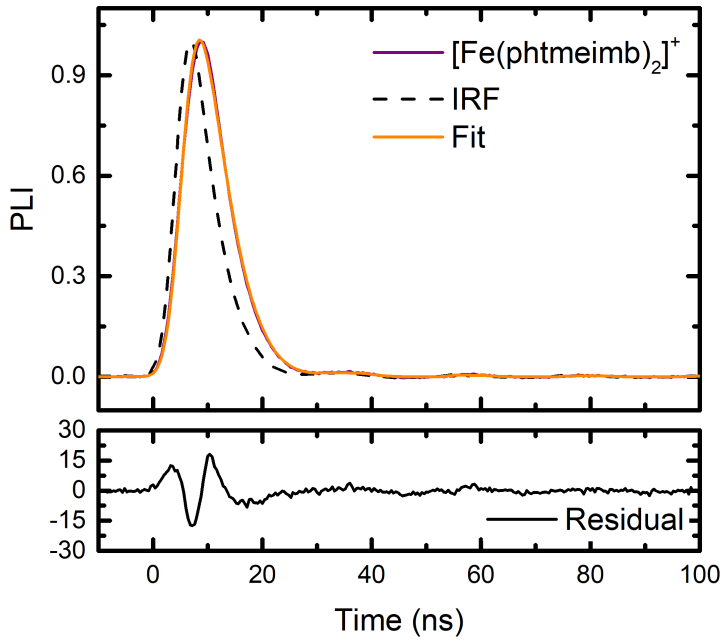

Figure S92. Reconvolution fitting used to fit the time-resolved PL data or $[Fe(phtmeimb)_2]^+$ recorded in argon-purged acetonitrile containing 0.1M $TBABF_4$. The bottom plot shows the residual of this fit.

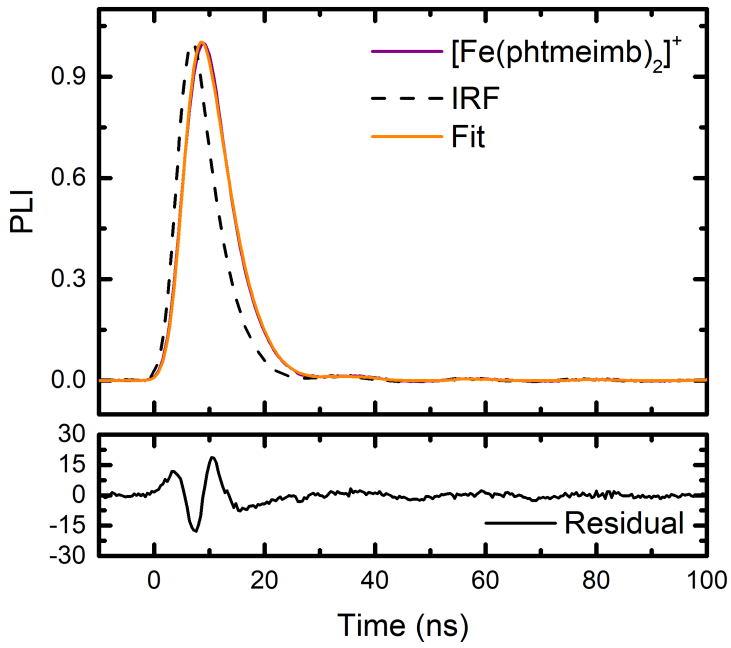

Figure S93. Reconvolution fitting used to fit the time-resolved PL data or $[Fe(phtmeimb)_2]^+$ recorded in air-equilibrated acetonitrile containing 0.1M $TBABF_4$. The bottom plot shows the residual of this fit.

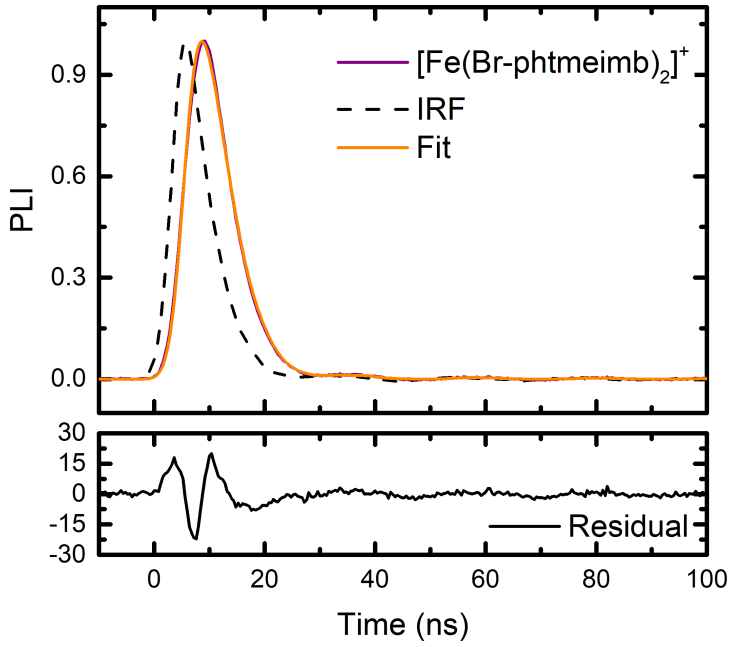

Figure S94. Reconvolution fitting used to fit the time-resolved PL data or $[Fe(Br\text{-}phtmeimb)_2]^+$ recorded in argon-purged acetonitrile containing 0.1M $TBABF_4$. The bottom plot shows the residual of this fit.

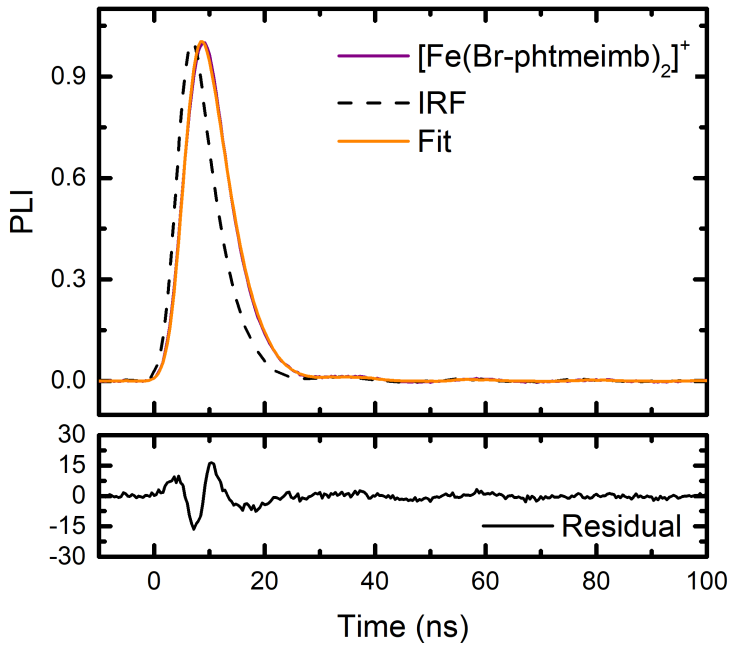

Figure S95. Reconvolution fitting used to fit the time-resolved PL data or $[Fe(Br\text{-}phtmeimb)_2]^+$ recorded in air-equilibrated acetonitrile containing 0.1M $TBABF_4$. The bottom plot shows the residual of this fit.

Characterization

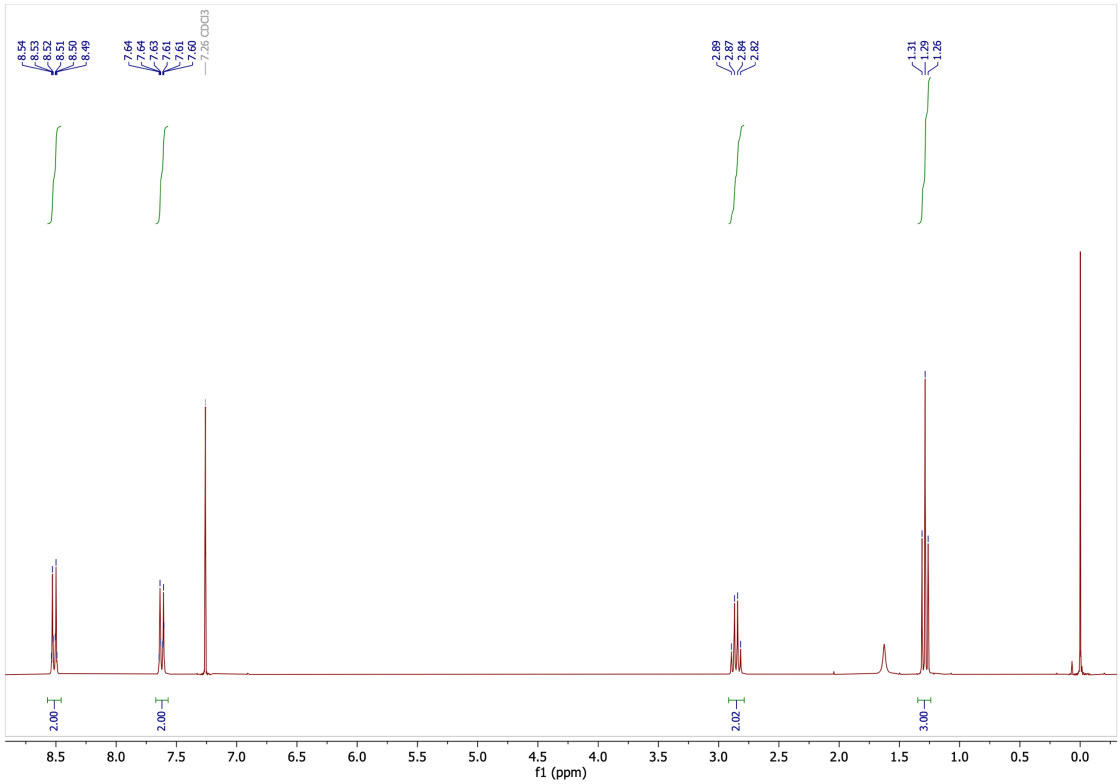

Figure S96. ^{1}H NMR spectra of 4-ethyl-benzene diazonium tetrafluoroborate recorded in $CDCl_3$ at 300 MHz at 298K.

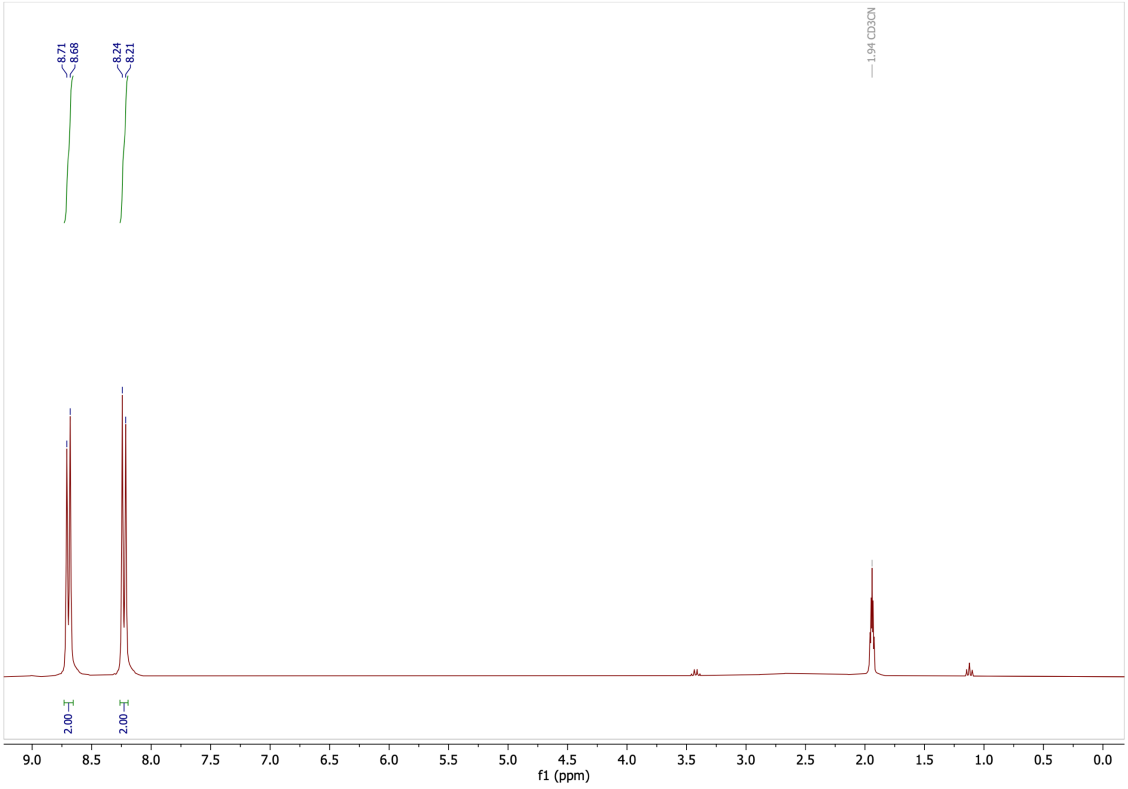

Figure S97. ^{1}H NMR spectra of 4-CF_3-benzene diazonium tetrafluoroborate recorded in CD_3CN at 300 MHz at 298K.

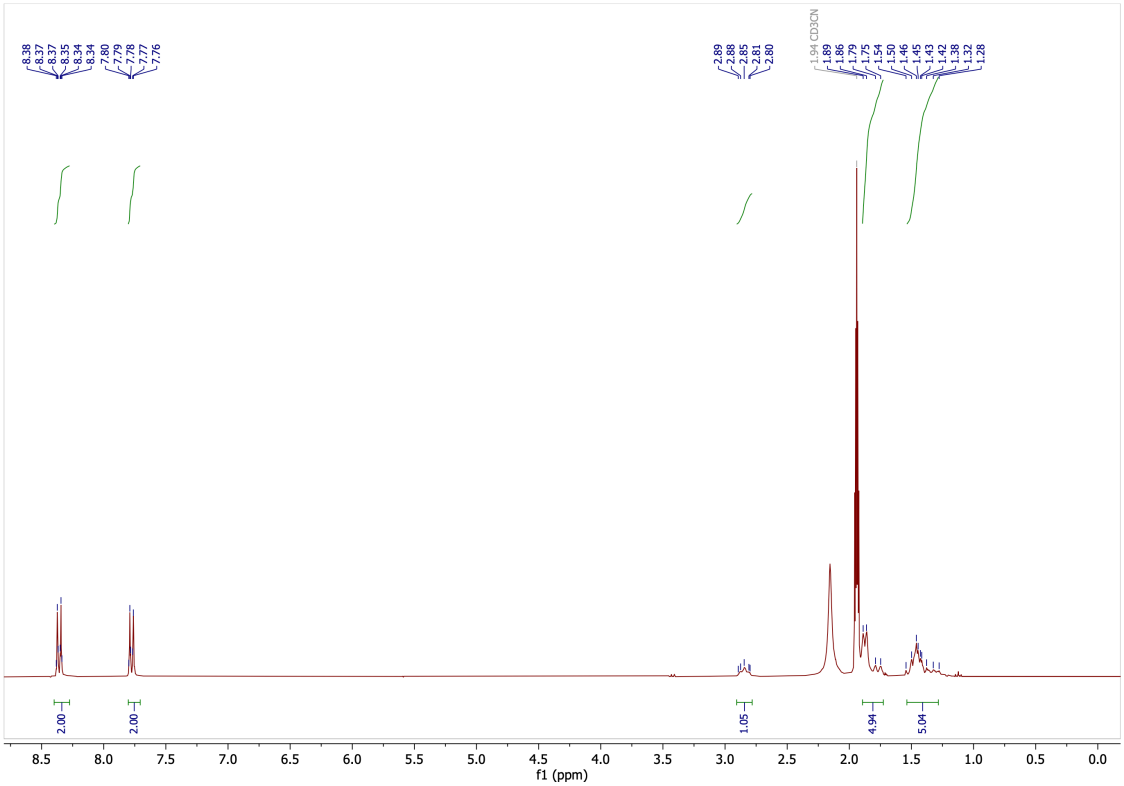

Figure S98. ^{1}H NMR spectra of 4-cyclohexyl-benzene diazonium tetrafluoroborate recorded in CD_3CN at 300 MHz at 298K.

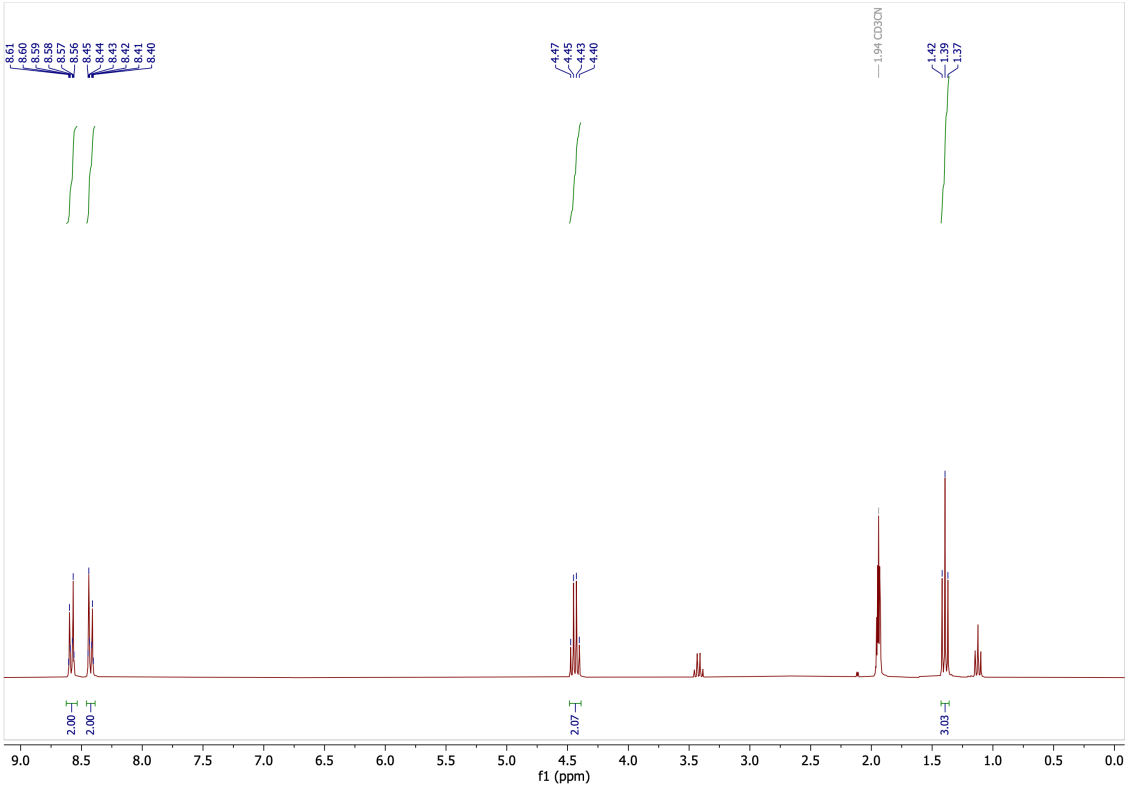

Figure S99. ^{1}H NMR spectra of 4-ethylester-benzene diazonium tetrafluoroborate recorded in CD_3CN at 300 MHz at 298K.

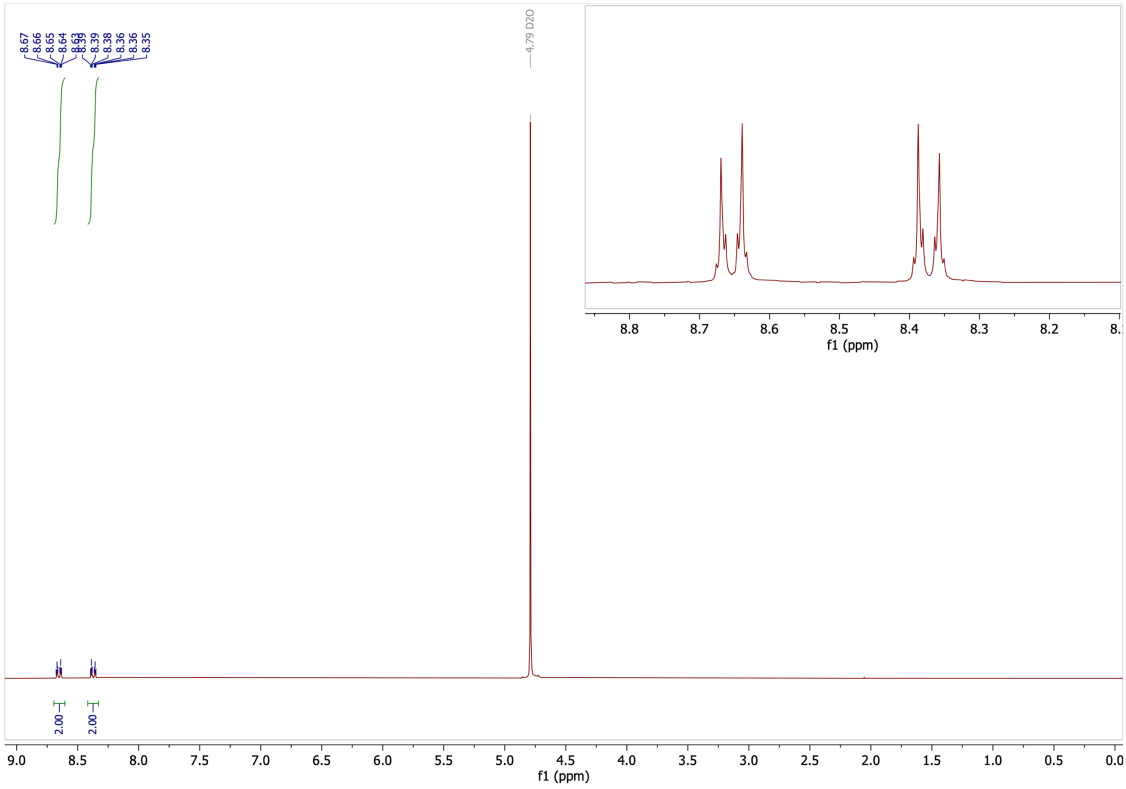

Figure S100. [1]H NMR spectra of 4-carboxylate-benzene diazonium tetrafluoroborate recorded in D_2O at 300 MHz at 298K.

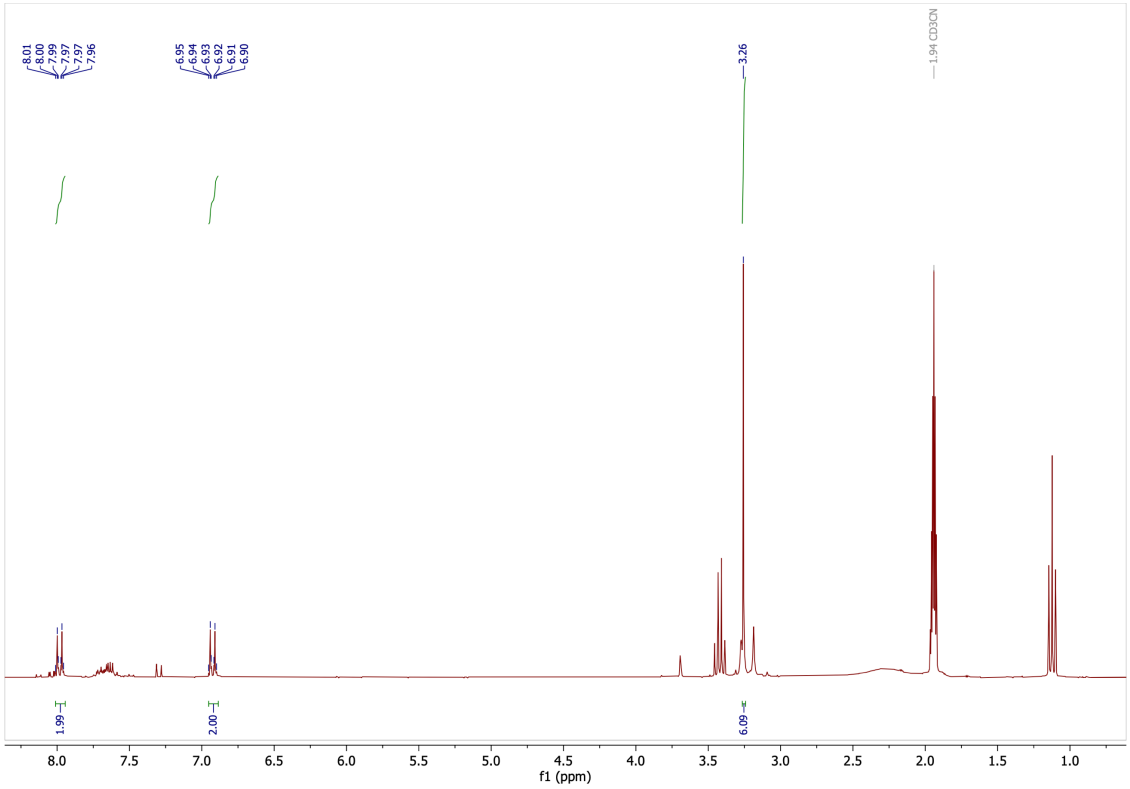

Figure S101. [1]H NMR spectra of 4-N,N-dimethylamino-benzene diazonium tetrafluoroborate recorded in CD_3CN at 300 MHz at 298K.

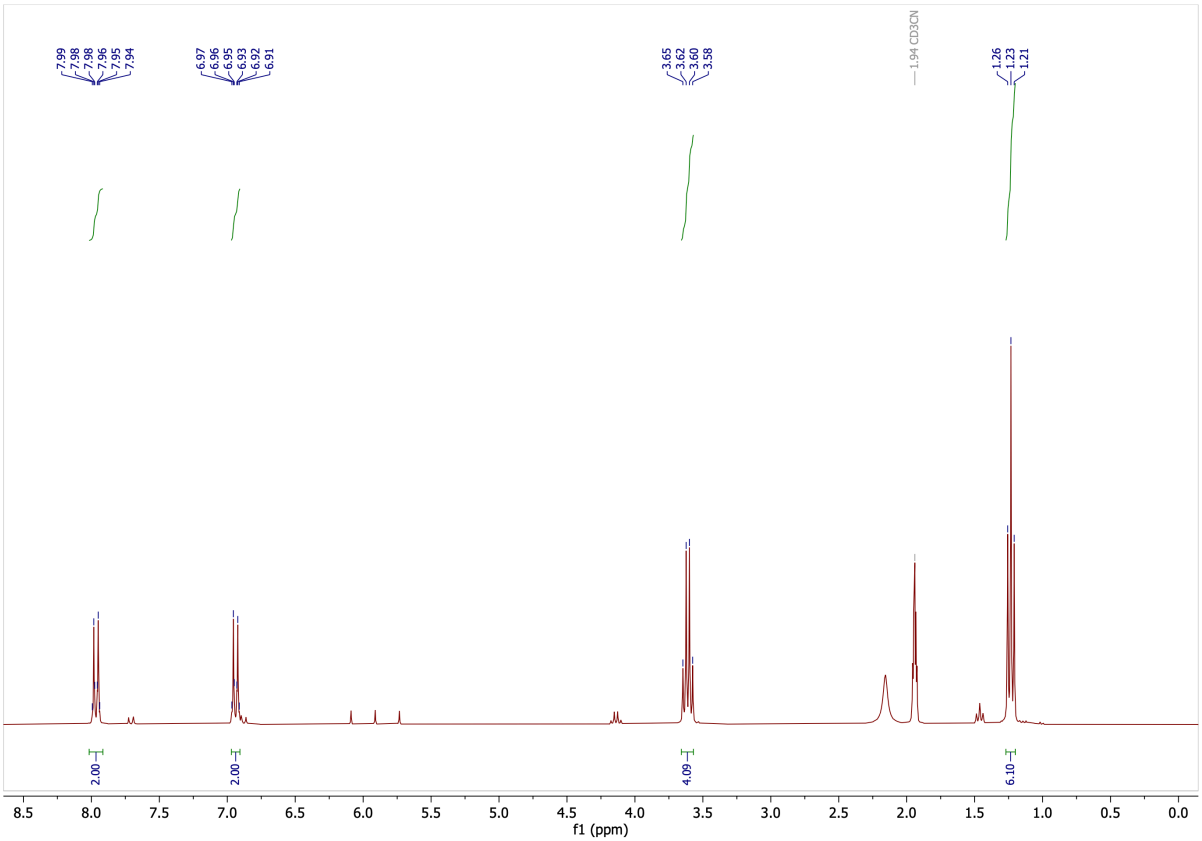

Figure S102. ^{1}H NMR spectra of 4-N,N-diethylamino-benzene diazonium tetrafluoroborate recorded in CD_3CN at 300 MHz at 298K.

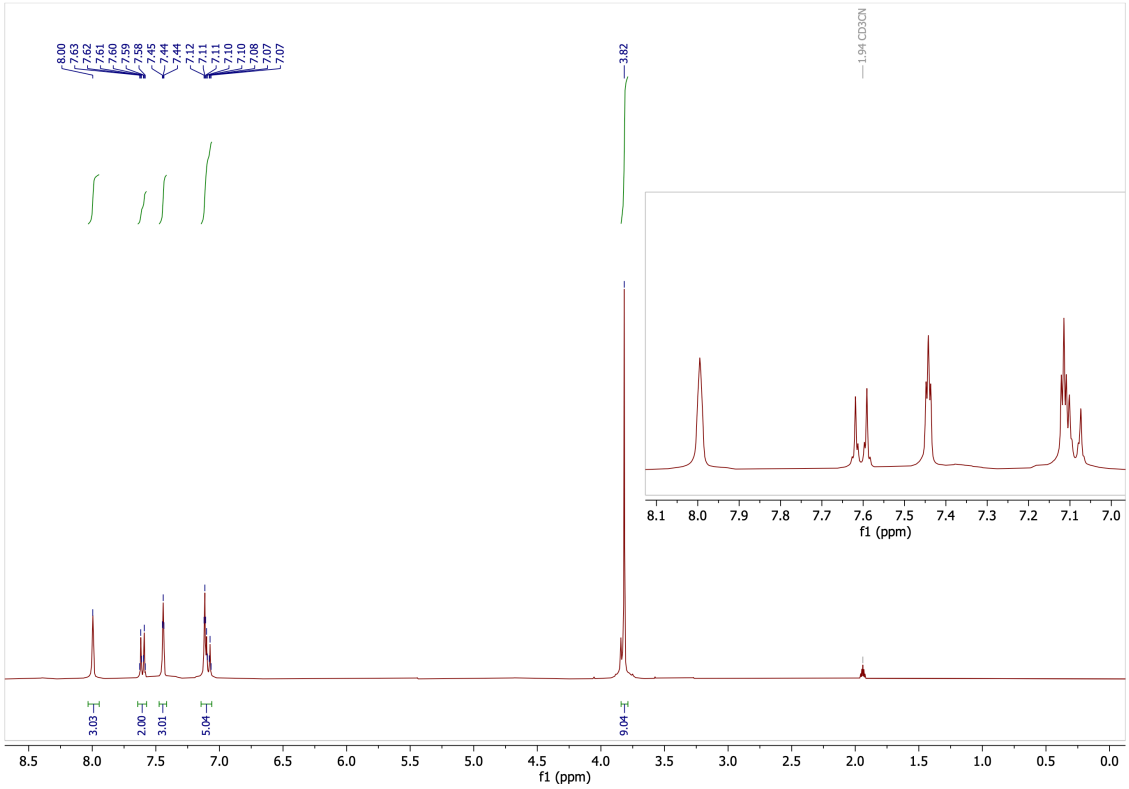

Figure S103. ^{1}H NMR spectra of tris(3-methylimidazolium-1-yl)(4-Br-phenyl)borate bis(hexafluorophosphate) recorded in CD_3CN at 300 MHz at 298K.

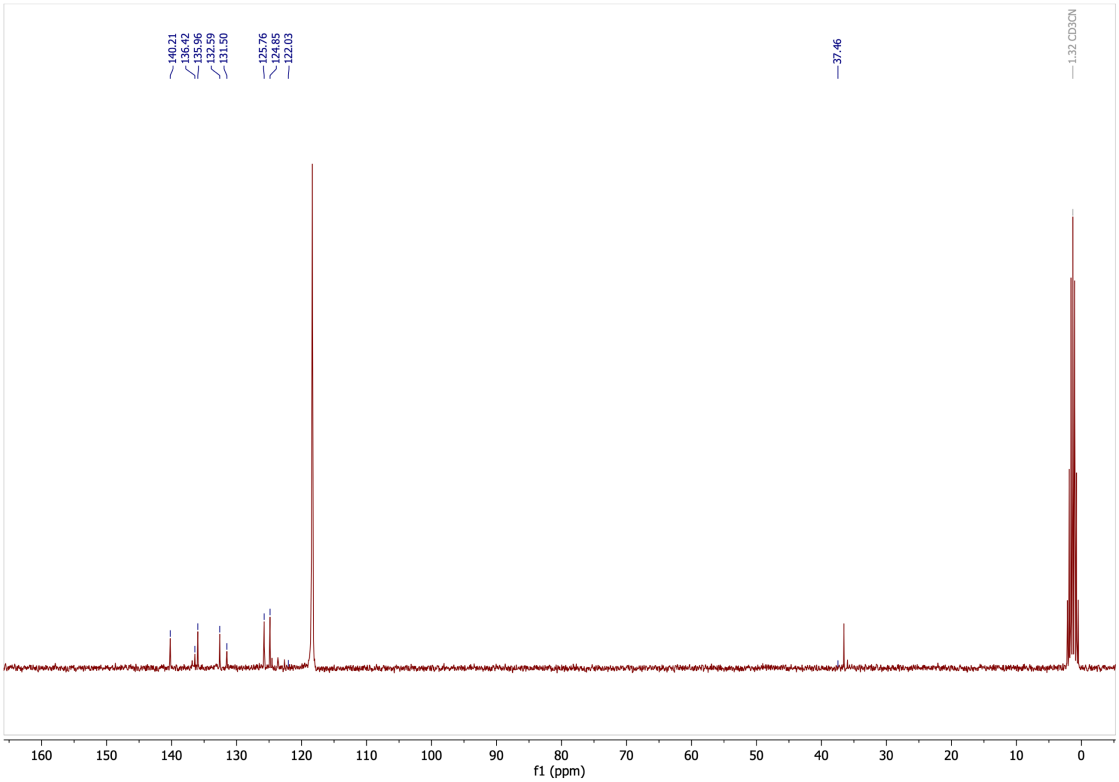

Figure S104. ^{13}C NMR spectra of tris(3-methylimidazolium-1-yl)(4-Br-phenyl)borate bis(hexafluorophosphate) recorded in CD_3CN at 75 MHz at 298K.

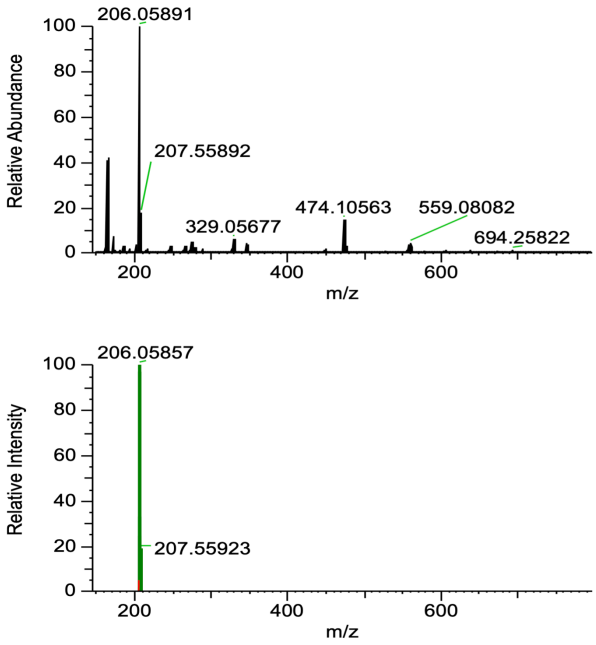

Figure S105. HRMS of tris(3-methylimidazolium-1-yl)(4-Br-phenyl)borate bis(hexafluorophosphate)

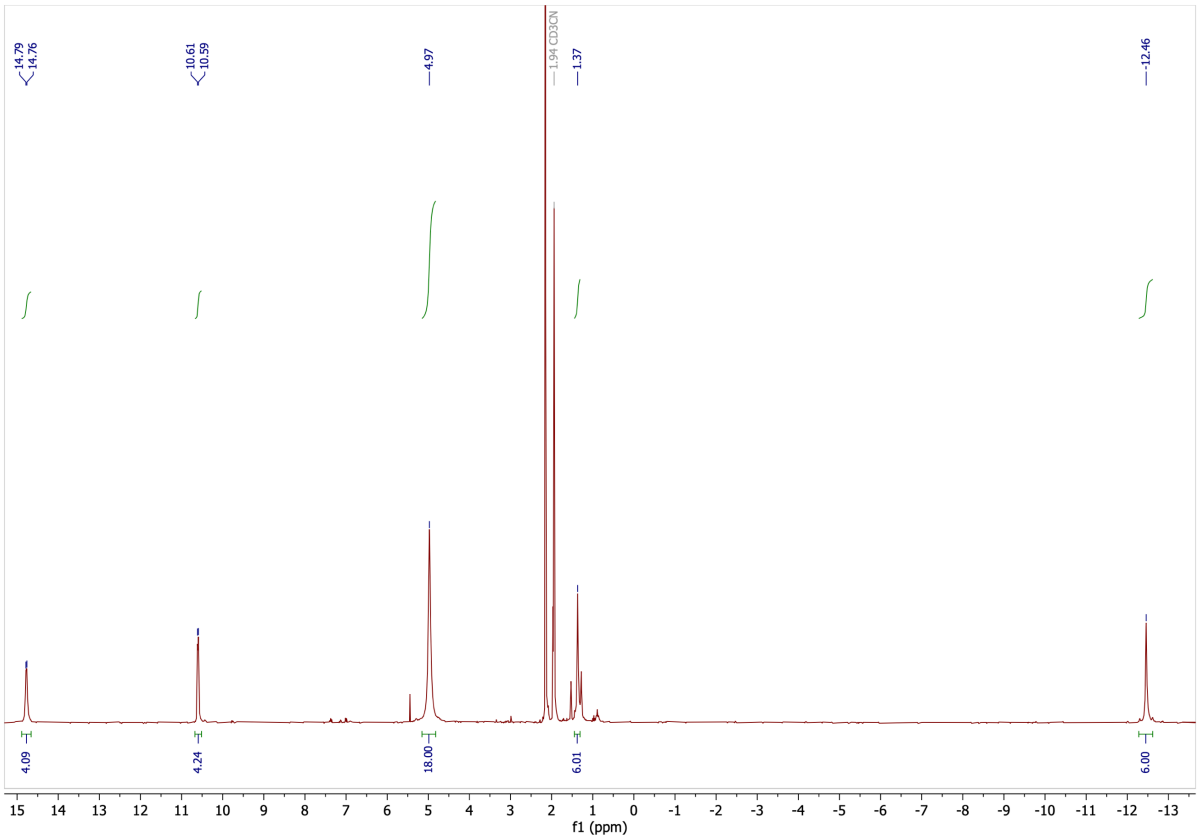

Figure S106. ^{1}H NMR spectra of $[Fe(Br\text{-}phtmeimb)_2]^{+}.PF_6^{-}$ recorded in CD_3CN at 300 MHz at 298K.

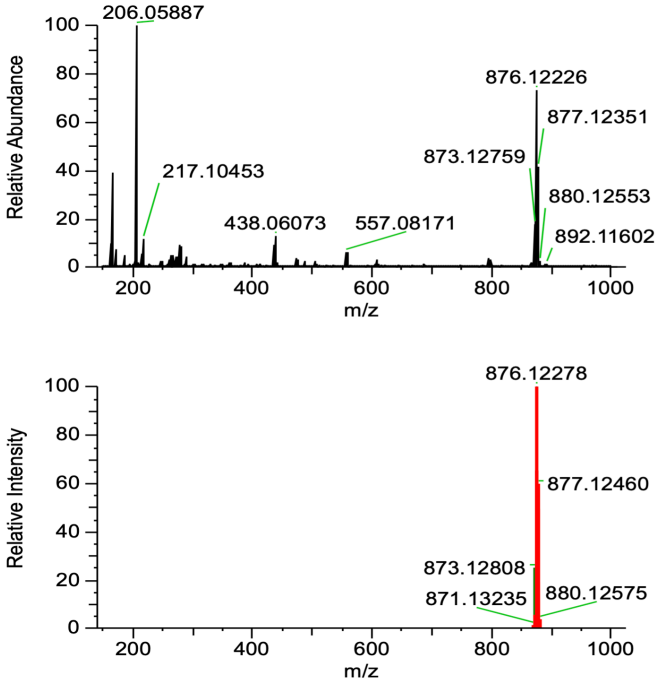

Figure S107. HRMS spectra of $[Fe(Br\text{-}phtmeimb)_2]^+.PF_6^-$

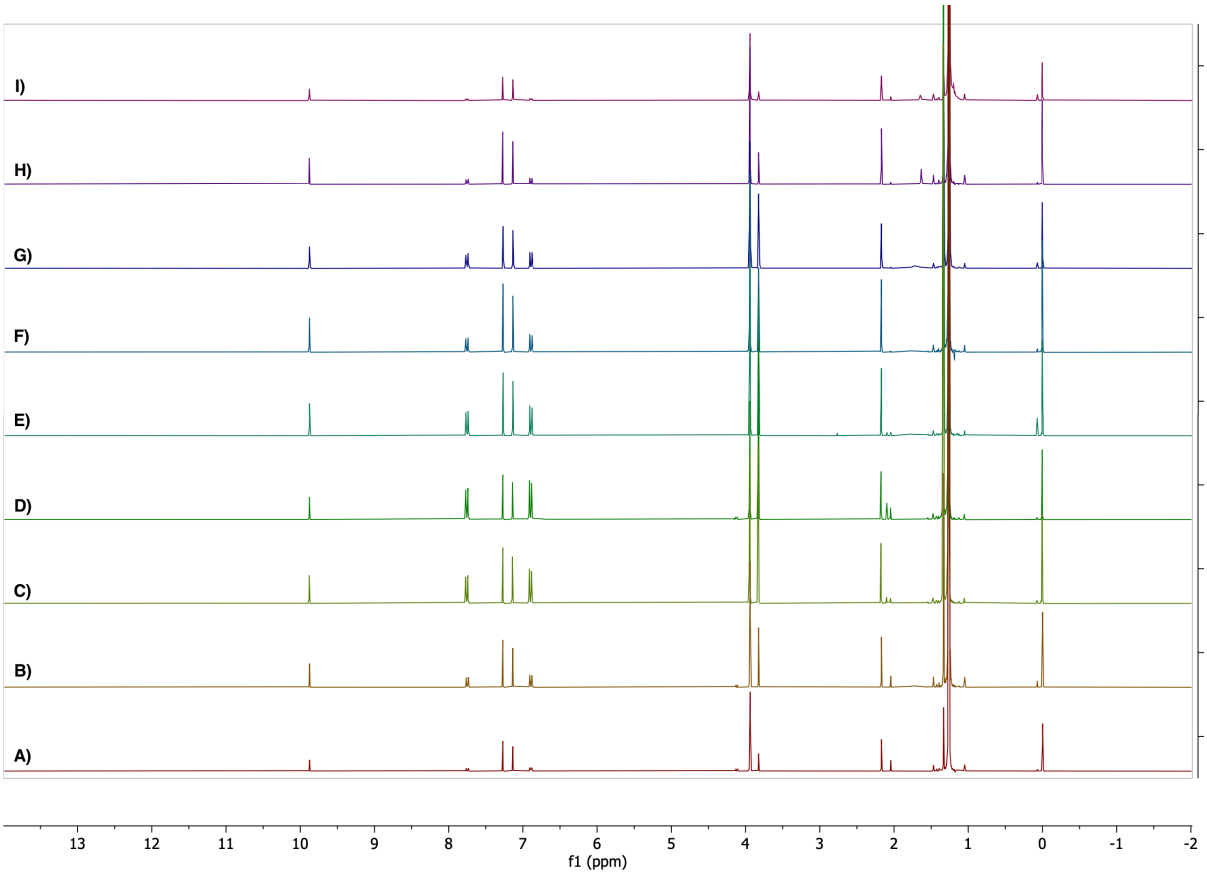

Figure S108. ^{1}H NMR (CDCl3, 300MHz, 298K) spectra for the C-B bond formation reactions using $[Cu(bcp)_2]^+$ (A), $[Fe(phtmeimb)_2]^+$ (B), $[Ir((dFCF_3)ppy_2)(dtb)]^+$ (C), $[Ir(ppy)_2(dtb)]^+$ (D), $[Ir(ppy)_3]$ (E), $[Os(bpy)_3]^{2+}$ (F), $[Ru(bpy)_3]^{2+}$ (G), $[Fe(Br\text{-}phtmeimb)_2]^+$ (H) and $[Cu(bcp)(DPEPHos)]^+$ (I) as photosensitizers. The crude reaction was first filtered on silica using ethyl acetate as eluent. 3,4,5-trimethoxybenzaldehyde was used as internal reference to estimate the reaction yields.

Electrochemistry

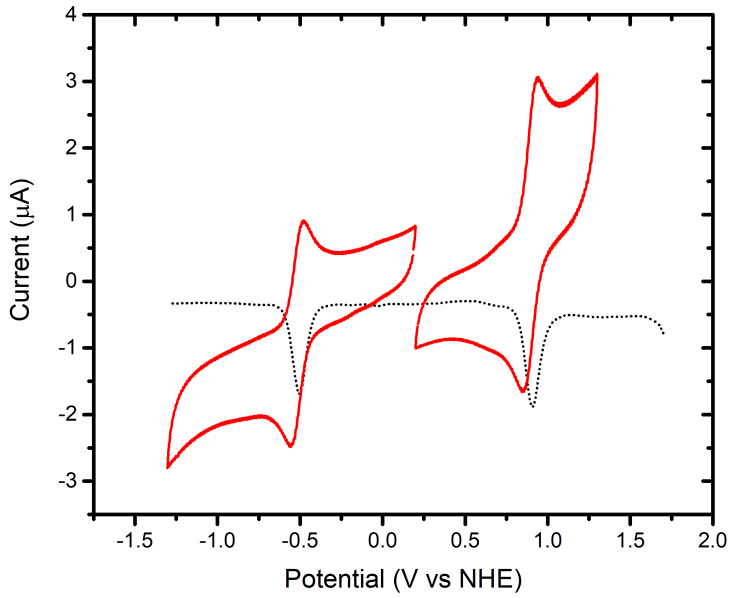

Figure S109. Cyclic (red) and differential pulse voltammetry (black dots) of $[Fe(Br\text{-}phtmeimb)_2]^+$ recorded in argon purged acetonitrile containing 100 mM $TBAPF_6$ electrolyte. A scan rate of 100 mV/s was used for cyclic voltammetry experiments.

Dark Reactivity

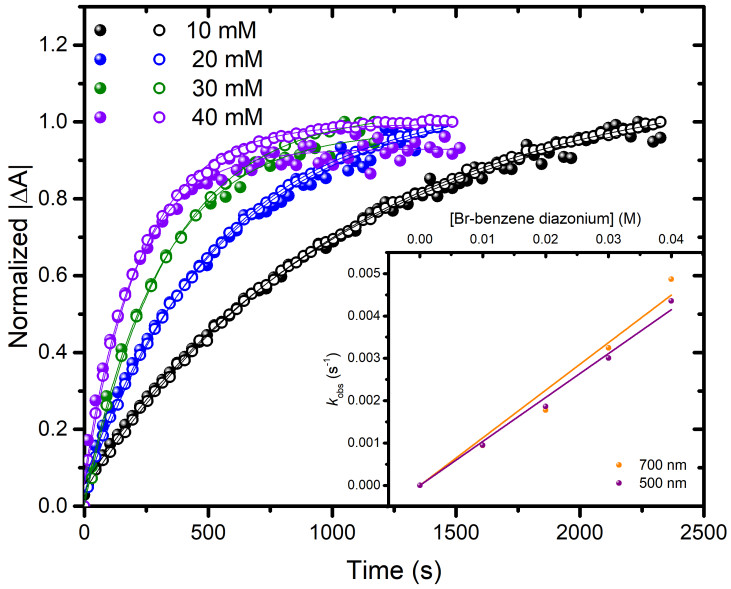

Figure S110. Normalized absolute absorption changes recorded at 700 nm (closed symbols) or 500 nm (open symbol) in acetonitrile at selected time intervals for a solution of $[Fe(phtmeimb)_2]^+$ (230 mM) in the presence of 10-40 mM 4-Br-benzene diazonium. The inset shows the observed rate at each concentration that was used to determine the rate constant for electron transfer.